IOP Publishing Journal of Physics D: Applied Physics

J. Phys. D: Appl. Phys. **47** (2014) 013001 (25pp) doi:10.1088/0022-3727/47/1/013001

Topical Review

Mechanical properties of nanoparticles: basics and applications

Dan Guo, Guoxin Xie and Jianbin Luo

State Key Laboratory of Tribology, Department of Mechanical Engineering, Tsinghua University, Beijing 100084, People's Republic of China

E-mail: guodan26@mail.tsinghua.edu.cn

Received 28 August 2013, revised 14 October 2013
Accepted for publication 24 October 2013
Published 3 December 2013

Abstract

The special mechanical properties of nanoparticles allow for novel applications in many fields, e.g., surface engineering, tribology and nanomanufacturing/nanofabrication. In this review, the basic physics of the relevant interfacial forces to nanoparticles and the main measuring techniques are briefly introduced first. Then, the theories and important results of the mechanical properties between nanoparticles or the nanoparticles acting on a surface, e.g., hardness, elastic modulus, adhesion and friction, as well as movement laws are surveyed. Afterwards, several of the main applications of nanoparticles as a result of their special mechanical properties, including lubricant additives, nanoparticles in nanomanufacturing and nanoparticle reinforced composite coating, are introduced. A brief summary and the future outlook are also given in the final part.

(Some figures may appear in colour only in the online journal)

1. Introduction

Nanoparticles, microscopic objects with at least one dimension less than 100 nm [1], have attracted intensive scientific attention. Distinctive size-dependent properties of nanoparticles often exist, which are mainly due to their relatively large surface area [2]. Moreover, when the size of a particle approaches nanoscale with the characteristic length scale close to or smaller than the de Broglie wavelength of the charge carrier (electrons and holes) or the wavelength of light, the periodic boundary conditions of the crystalline particle are destroyed, or the atomic density on the amorphous particle surface is changed [3]. Due to these, a lot of the physical properties of nanoparticles are quite different from bulk materials, yielding a wide variety of new applications. For example, nanoparticles encapsulated or adsorbed in matrix materials have been used as carriers for delivering drug molecules [1, 4, 5]. Stability, self-assembly behaviour and mutual interactions of nanoparticles at fluid interfaces are very relevant to many colloid applications [6]. Special optical properties due to the excitation of surface plasmons in metallic nanoparticles can be used in biomedicine, energy and environment protection technologies [7]. Magnetic nanoparticles could become superparamagnetic and respond to external magnetic fields very fast with almost zero remanence [8]; these properties lay bases for applications such as biomedical imaging and information storage technology [9, 10]. Some of the basic functions of nanoparticles, e.g., a catalysis of electrochemical reactions and the enhancement of electron transfer, make them very useful in designing novel electrochemical sensing systems [11].

As such, research topics on the mechanical properties of nanoparticles have become increasingly hot in recent years; the number of relevant publications has increased dramatically, as shown in figure 1. Nanoparticles show different mechanical properties relative to microparticles and bulk materials, providing more effective options for the surface modification of many devices in the mechanical strength, or to improve the quality of nanomanufacturing/nanofabrication, etc. To be more specific, on the one hand, the mechanical effects of nanoparticles can affect the tribological properties of lubricants with nanoparticles [12] as well as reinforce composite coatings [13]. In a lubricated contact, the comparison in the hardness between nanoparticles and the contacting surface determines whether particles are deformed or indented into the surface when the contact pressure is sufficiently large [14]. This

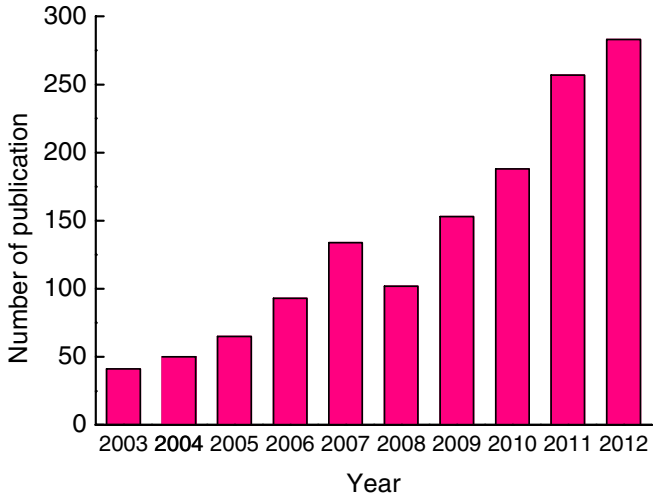

Figure 1. The number of publications related with the topic on the mechanical properties of nanoparticles in the past decade.

information could reveal how the particles behave in the contact. On the other hand, nanoparticles are usually used as abrasives in the nanopolish of ultra-smooth surfaces by chemical mechanical polishing (CMP), which is the most effective planarization tool in the manufacture of an integrated circuit (IC), till now. Good controls over the mechanical properties of particles and their interactions with the polished surface etc are important for improving the surface quality and enhancing material removal [15, 16]. Successful applications in these fields usually need a deep understanding of the basics of the nanoparticles' mechanical properties, such as hardness and elastic modulus, interfacial adhesion and friction, movement law, as well as their size-dependent effects. In order to acquire more of this information, different testing methods have been developed, e.g., nanoindentation with atomic force microscopy (AFM) [17, 18], *in situ* compression by a force probing holder based on the observation with transmission electron microscopy (TEM) [19, 20]. However, the obtained results are still inadequate and some are controversial. For instance, there is still no definite conclusion as to whether the elastic modulus of nanoparticles measured with AFM is affected by the particle size and the indentation depth [21–24]. Furthermore, the contact mechanics, especially the frictional and mechanical behaviours related to nanoparticles, have not been fully understood. The applicability of classic theories, e.g., the Hertzian theory, for describing the contact behaviours in the case of particle sizes down to the nanoscale, is still in discussion [23, 24].

This work aims at giving a review of the important recent advances in the mechanical properties of nanoparticles, from the basics to their application. The review is organized into four sections: section 1 discusses the mechanical models and theories between nanoparticles or the nanoparticles acting on a surface. In this part, the basic concepts of the relevant interfacial forces and theories of nanoparticles, e.g., the van der Waals force, electrostatic force, capillary force, DLVO theory, contact and adhesion theories etc are also introduced. Section 2 briefly describes some of the typical measurement techniques currently used for studying the mechanical properties of nanoparticles. Section 3 summarizes the important results on some of the mechanical properties of nanoparticles, such as hardness, elastic modulus, adhesion and friction, as well as movement. Section 4 introduces the main applications of nanoparticles that result from their special mechanical properties; these applications include a lubricant with nanoparticles as additives, nanoparticles in nanomanufacturing and nanoparticle reinforced composite coating. The general framework of this review is schematically given in figure 2.

2. Interaction forces and basic theories relevant to the mechanical properties of nanoparticles

'As we go down in size, there are a number of interesting problems that arise.'—Feynman [25]. The first problem is the diverse interaction forces between the nanoparticles themselves, or between them and the surface.

2.1. Van der Waals (vdW) forces

VdW forces are the weak interaction between all molecules and particles, which play important roles in the particles' mechanical properties. This kind of force includes three parts: one is the orientation force (the Keesom force) [26], resulting from the interaction between the permanent dipole moment of polar molecules. The second is the induction force (the Debye force) [27], which comes from the interaction between the permanent dipole moment of the polar molecule and the induced dipole moment. The third is the dispersion force (the London force) [28], which exists in a wide variety of polar and nonpolar molecules, coming from the induced instantaneous dipole polarization. VdW energies are usually from several to dozens of thousands of Joules per mole, one or two orders of magnitude smaller than the chemical bond energy. The vdW forces are long-range forces and can be effective in a large range of distances, varying from long distances greater than 10 nm down to atomic scale distance (about 0.2 nm) [29]. The methods for calculating the vdW interaction forces or energies between small molecules or large macroscopic bodies have been well established [29]. Several of the common vdW forces and energies are given in table 1. The vdW forces of objects with any shape can be transformed with the Derjaguin approximation to those between two planes per unit area [30]. Based on the quantum electrodynamics theory, Lifshitz deduced the expression for calculating Hamaker constants, which can be used to solve problems with media involved [32]. Typically, the Hamaker constants for interactions in a medium are an order of magnitude lower than those in a vacuum [33]. The vdW force is always attractive between identical materials, but it may be repulsive between dissimilar materials in a third medium (usually liquid) [29].

2.2. Electrostatic force and electrical double layer (EDL) force

For particles suspended in water or any liquid with a high dielectric constant, they are usually charged and can be prevented from coalescing due to the repulsive electrostatic force. The charging of a surface in a liquid has three main

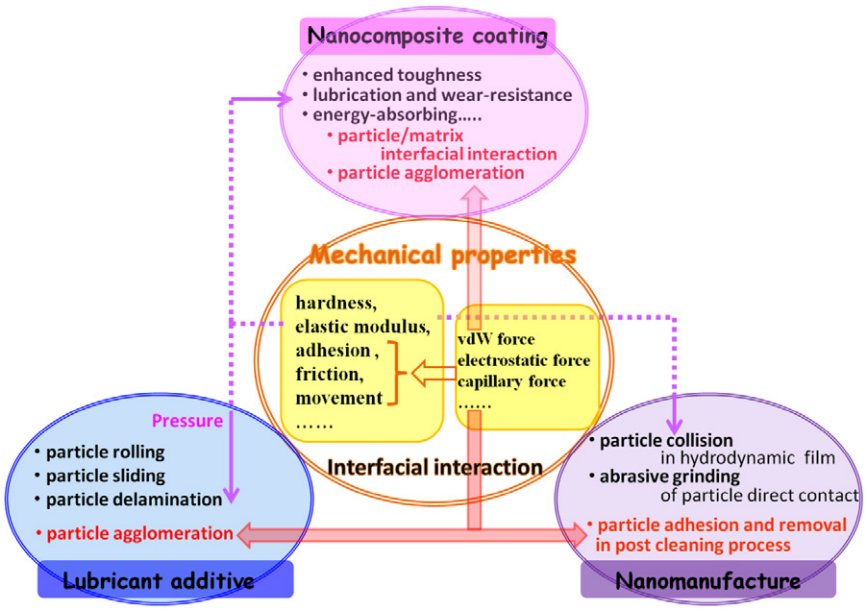

Figure 2. Schematic diagram of the framework of this review.

Table 1. Several of the common vdW energies and forces.

Types	vdW energies	vdW forces
Molecular-plane	$W = -\frac{\pi C_{\mathrm{vdW}}\rho}{6D^3}$	$F = -\frac{\pi C_{\mathrm{vdW}}\rho}{2D^4}$
Sphere–sphere	$W = -\frac{A}{6D}\frac{R_1R_2}{R_1+R_2}$	$F = -\frac{A}{6D^2}\frac{R_1R_2}{R_1+R_2}$
Sphere–plane	$W = -\frac{AR}{6D}$	$F = -\frac{AR}{6D^2}$
Plane–plane	$W = -\frac{A}{12\pi D^2}$	$F = -\frac{A}{6\pi D^3}$

Note: C_{vdw} is a coefficient related to the atomic pair potential, R is the sphere radius, R_1 and R_2 are the radii of two spheres, respectively, D is the distance between two surfaces, $A = \pi^2 C_{\mathrm{vdW}}\rho_1\rho_2$ is the Hamaker constant [31] and ρ is the atomic density.

sources [29]: (1) the ionization or dissociation of surface groups; (2) the adsorption or binding of ions from the solution onto a previously uncharged surface; (3) when two dissimilar surfaces are very close, charges can hop across from one surface to the other. The surface charges are balanced by an oppositely charged ion layer in the solution at some distance away from the surface, forming the EDL. The idea of the EDL was first formally proposed by Helmholtz, who derived the charge distribution in the solution based on the simple molecular capacitor model [34]. In reality, the thermal motion of ions in the solution introduces a certain degree of chaos causing the ions to be spread out in the region of the charged surface, forming a 'diffuse' double layer. In that case, the analysis of the electronic environment near the surface is more complex and requires more detailed analyses [33]. Gouy [35], Chapman [36] and Stern [37] put forward more accurate models for analysing the surface and electrolyte interfaces, making great contributions to the development of EDL theories. Gouy [35] and Chapman [36] independently developed theories of a so called 'diffuse double layer', in which the change in the concentration of the counter ions near a charged surface follows the Boltzmann distribution. The Gouy–Chapman theory provides a better approximation of the real system than the Helmholtz theory, but it still has limited quantitative applications. It assumes that ions behave as point charges and that there is no physical limit for the ions in their approach to the surface. Then, the Gouy–Chapman diffuse double layer was modified by Stern [37] so that ions have a finite size and cannot approach the surface closer than a few nanometres: the first layer of ions in the Gouy–Chapman diffuse double layer are not at the surface, but at some distance away from the surface. As a result, the potential and concentration of the diffuse part of the layer is low enough to justify treating the ions as point charges. Stern also assumed that some ions are probably adsorbed by the surface in a plane; this layer is known as the 'Stern layer' [37]. Within this layer, thermal diffusion is not strong enough to overcome the electrostatic forces. In the diffusive outer layer, the ions are far enough from the solid surface and are subjected to weak electrostatic forces from the surface only, hence they remain mobile.

A double layer is formed to neutralize the charged surface, which in turn causes an electrokinetic potential between the surface and any point in the mass of the suspending liquid. This voltage difference is of the order of millivolts and is referred to as the surface potential. The magnitude of the surface potential is influenced by the surface charge and the thickness of the double layer. Starting from the surface, the potential drops off roughly linearly in the Stern layer and then exponentially through the diffuse layer, approaching zero at the imaginary boundary of the double layer. The potential curve is useful because it can suggest the electrical force strength between particles and the critical distance within which this force comes into play. A charged particle's mobility is related to the dielectric constant and the viscosity of the suspending liquid, as well as the zeta potential, which is a potential at the boundary between the moving particle and the liquid. The

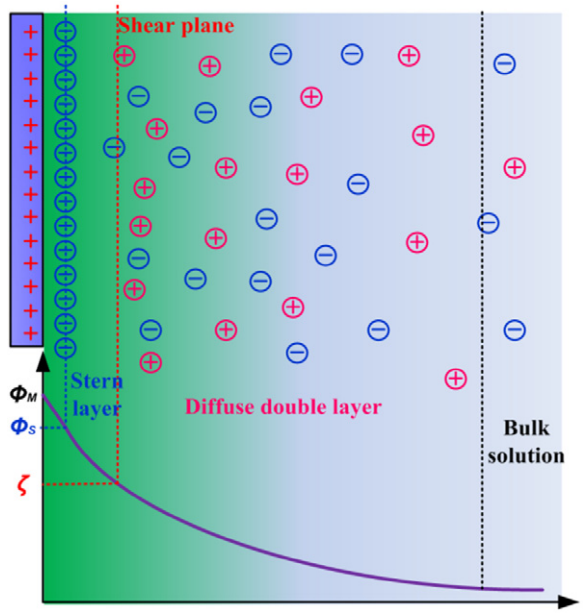

Figure 3. Schematic model of EDL.

boundary is called the slip plane and usually defined as the point where the Stern layer and the diffuse layer meet [38, 39]. The common EDL model is shown in figure 3. The EDL interaction energy and the force between the bodies of different geometries can be referred to [40].

2.3. Capillary force

Capillary force is mainly due to the formation of liquid menisci (also termed the meniscus force), the significance of which was realized by Haines [41] and Fisher [42]. Capillary force can be classified into two types: normal capillary force and lateral capillary force [43]. A comprehensive review of the normal capillary force was given by Butt and Kappl [44]. Denkov *et al* [45] and Kralchevsky and Nagayama [46] contributed a lot to the study of the structure of colloid nanoparticles due to the lateral capillary force. Capillary forces should be considered in the studies on powders, soils and granular materials [47–50], the adhesion between particles or particles to surfaces [51, 52] and the stiction in micro/nano-electromechanical systems [53]. It is also relevant to nanoparticle assembling or living cells self-assemble technologies [54, 55].

The normal capillary force arises from the Laplace pressure within the curved meniscus formed by liquid condensation or vapour bridges around two adhering solid surfaces [43, 44]. It can be attractive or repulsive depending on whether the capillary bridge is concave or convex. Two equations are important to understand the capillary forces, i.e. the Young–Laplace equation and the Kelvin equation. The Young–Laplace equation relates the curvature of a liquid interface to the pressure difference, while the Kelvin equation describes capillary condensation, which is the physical basis for many adhesion phenomena [46]. Capillary condensation is the condensation of vapour into capillaries or fine pores even for vapour pressures below the saturation vapour pressure. The Kelvin equation relates the actual vapour pressure to the surface curvature of the condensed liquid. The normal capillary force is owing to two actions: one is the pressure difference across the curved interface and the other is the action of the surface tension force exerted around the annulus of the meniscus. Butt and Kappl [44] gave the usual derivations and expressions for capillary forces between different geometries.

The origin of the lateral capillary forces is the overlap of the perturbations in the shape of a liquid surface due to the presence of attached particles [46]. The larger the interfacial deformation created by the particles, the stronger the capillary interaction between them. The theories and expressions of lateral capillary forces for particles bound to interfaces, liquid films and biomembranes were included in a good review by Kralchevsky and Nagayama [46]. The lateral capillary forces are effective in controlling small colloidal particles and protein macromolecules confined in liquid films to form fine microstructures.

2.4. Other forces—solvation, structural and hydration forces

Apart from vdW forces and EDL forces, some other forces, i.e. solvation, structural or hydration forces, come into play when two surfaces or particles approach very close (separation less than a few nanometres) in the liquid. These forces can be monotonically repulsive, monotonically attractive or oscillatory and they can be much stronger than either the vdW forces or EDL forces at small separations. Solvation, structural or hydration forces (in water) arise between two particles or surfaces if the solvent or water molecules become ordered by the surfaces [56]. When the ordering occurs, an exponentially decaying oscillatory force with a periodicity equal to the size of the confined liquid molecules, micelles or nanoparticles appears [56–58]. Solvation forces depend not only on the properties of the liquid medium but also on the surface physicochemical properties, such as hydrophilicity, roughness, crystalline state, homogeneity, rigidity and surface micro-texture. These factors affect the structure of the confined liquids between two surfaces, which in turn affects the solvation force [29]. The hydration force is a strong short-range repulsive force between the polar surfaces separated by a thin polar liquid layer (thickness <3 nm); the force magnitude decays exponentially with the liquid layer thickness [58–62]. The physical mechanisms underlying the hydration force are still in discussion. A well known interpretation of hydration force is that the solvent molecules are bound strongly and are restructured by polar surfaces. An ordered-solvent layer was formed at the surface-solution interface, which exponentially decays away from the surface; the overlap of the ordered-solvent layers near the two mutually approaching surfaces creates a force [59–61]. The hydration force could determine the behaviours of many diverse systems, e.g., the colloidal dispersion stability, the swelling of clays and the interactions of biological membranes.

2.5. DLVO theory

The DLVO (Derjaguin–Landau–Verwey–Overbeek) theory was introduced by Derjaguin and Landau [63] in 1941 and Verwey and Overbeek [64] in 1948 for describing the stability

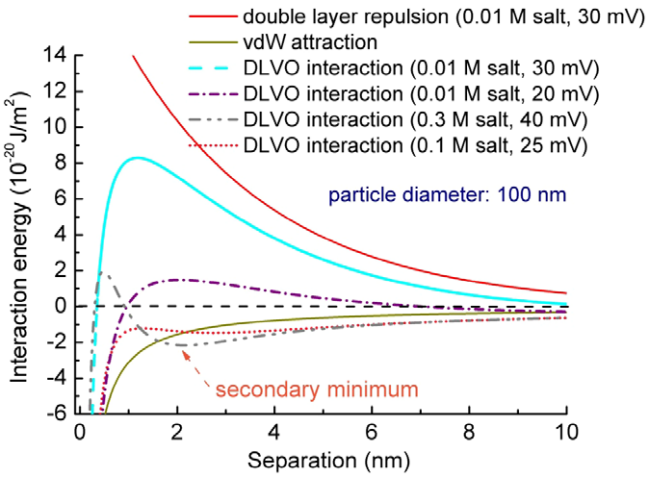

Figure 4. Schematic plots of the DLVO interaction potential energy E (the Hamaker constant A is 1.5×10^{-20} J).

of colloidal dispersions. The theory combines the effects of the vdW attraction and the electrostatic repulsion. It can explain many phenomena quantitatively in colloidal science, e.g., the adsorption and the aggregation of nanoparticles in aqueous systems, and describe the force between charged surfaces interacting through a liquid medium [65–69]. Figure 4 shows the schematic plot of the DLVO interaction potential energy E of model nanoparticles (diameter: 100 nm and surface potential: 20–40 mV) which are dispersed in aqueous salt solutions.

It can be seen that a strong long-range repulsion with a high energy barrier is present for highly charged surfaces in dilute electrolyte (i.e. long Debye length). When the surface charges are reduced or the concentration of the electrolyte solutions are increased, a small secondary minimum in the potential energy curve appears. Colloid particles may undergo a reversible flocculation due to the secondary minimum because of its weak energy barrier [33], resulting in slow particle aggregation for the surface with a low charge density. Below a certain surface charge or above a certain electrolyte concentration (known as the critical coagulation concentration), the energy barrier falls below the zero axis and particles then coagulate rapidly. Consequently, the colloid system becomes unstable.

Although the DLVO theory is the basis for understanding colloid stability and has a considerable amount of experimental support, it is inadequate for the colloid properties in the aggregated state. This is because short-range interactions are dominant in this state and the specific properties of ions should be taken into account rather than regarded as point particles. Most deviations of experimentally measured forces from those expected from the DLVO theory are due to the existence of a Stern-layer or non-DLVO forces, e.g., ion-correlation, solvation, hydrophobic and steric forces [70–72].

2.6. Contact, adhesion and deformation theories of nanoparticles

In traditional contact theories for two objects in contact with each other under external forces, for instance, the simplest case of two interacting elastic spheres deduced by Hertz in 1882 [73], surface forces were not included. In these models, the displacement and the contact area are equal to zero when no external force is applied. However, as the size of the object is decreased to the nanoscale, the surface forces play a major role in their adhesion, contact and deformation behaviours. Modern theories of the adhesion mechanics of two contacting solid surfaces are based on the Johnson–Kendall–Roberts (JKR) theory [74] or the Derjaguin–Muller–Toporov (DMT) theory [75]. The JKR theory is applicable to easily deformable, large bodies with high surface energies. Strong, short-range adhesion forces dominate the surface interaction; the effect of adhesion is included within the contact zone. In contrast, the DMT theory better describes very small and hard bodies with low surface energies [76]. In this case, the adhesion is caused by the presence of weak, long-range attractive forces outside the contact zone. Tabor [76] introduced a nondimensional physical parameter, often referred to as Tabor's parameter, to quantify the limits of JKR, DMT and the cases between them. The intermediate regime between the JKR and the DMT theories has also been described by Maugis [77] using the Dugdale model [78]; a 'transition parameter' roughly equivalent to Tabor's parameter was defined [77]. A summary of the different conventions used for defining the 'transition parameter' was given by Greenwood [79]. Carpick *et al* [80] provided a simple analytic equation to determine the value of the 'transition parameter'; it could closely approximate Maugis' solution. The expansion of the JKR theory by Maugis and Pollock [81] leads to the additional description of plastic deformation. Table 2 summarizes the relations between the contact radius, deformation and the adhesion force for two spheres contacting each other according to the three mostly used theories.

Although the Hertz, JKR and DMT theories have been widely used to study the mechanical properties of nanoparticles

Table 2. Relations between the contact radius a, the contact radius a_0 due to adhesion force without an external load, the deformation δ and the adhesion force for two spheres contacting each other according to the Hertz, JKR and DMT theories.

	Hertz	JKR	DMT
a	$\left(\frac{R^*P}{E^*}\right)^{1/3}$	$\left\{\frac{R^*}{E^*}[P+3\pi R^*\gamma + (6\pi R^*\gamma P + (3\pi R^*\gamma)^2)^{1/2}]\right\}^{1/3}$	$\left[\frac{R^*}{E^*}(P+2\pi R^*\gamma)\right]^{1/3}$
δ	$\frac{a^2}{R^*}$	$\frac{a^2}{R^*}$	$\frac{a^2}{R^*} - \left(\frac{8\pi a\gamma}{3E^*}\right)^{1/2}$
a_0	0	$\left(\frac{6\pi R^{*2}\gamma}{E^*}\right)^{1/3}$	$\left(\frac{2\pi R^{*2}\gamma}{E^*}\right)^{1/3}$
P_{ad}	0	$2\pi R^*\gamma$	$\frac{3\pi R^*\gamma}{2}$

Note: R^* is the reduced radius defined as $1/R^* = (1/R_1) + (1/R_2)$, γ is the adhesion work per unit area. P is the external force and E^* is the reduced Young's modulus defined as $(1/E^*) = \frac{3}{4}[((1-\nu_1^2)/E_1) + ((1-\nu_2^2)/E_2)]$, E_1, E_2, and ν_1, ν_2 are Young's moduli and Poisson's ratios of the two spheres, respectively.

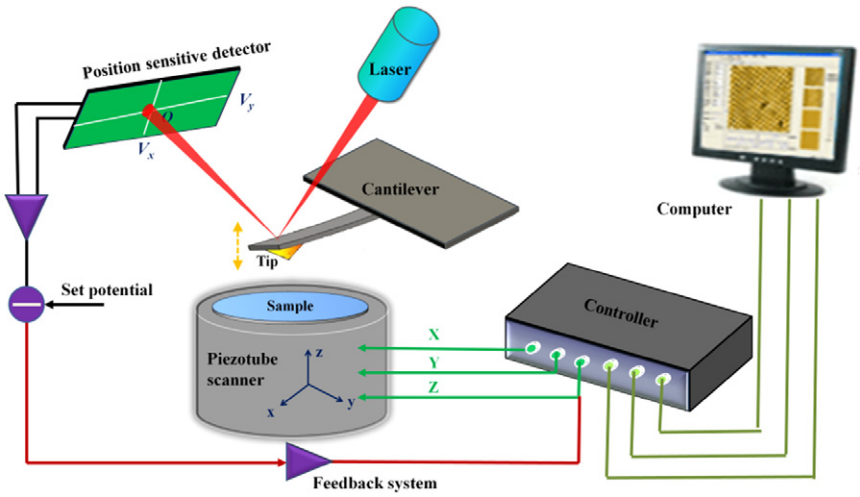

Figure 5. Schematic diagram of the basic working principle of AFM.

[21, 22, 82, 83], whether or not the continuum mechanics can be used to describe a particle at the nanometre scale is still in discussion. The molecular dynamics (MD) simulation method provides an opportunity to understand the atomistic processes in the contact region. Luan and Robbins [84] researched the contact between two nanocylinders by MD simulations and found that the atomic-scale surface roughness produced by discrete atoms led to dramatic deviations from the continuum theory. Contact areas and stresses may be changed by a factor of two, whereas friction and lateral contact stiffness by an order of magnitude. Also Miesbauer *et al* [85] analysed the contact between two NaCl nanocrystals with MD simulations. It was found that the Hertzian theory was a suitable description of the studied system when the system size was larger than 50 Å; the discrepancy became more obvious as the particle was even smaller. Cheng and Robbin [86] investigated the nanoscale contact with MD simulations to test the adaptability of continuum contact mechanics at the nanoscale; the results suggested that the continuum contact models could be applied to the case where the forces averaged over the areas containing many atoms. Nonetheless, the continuum theory, because of its concise expression, is still widely applied in the mechanical analysis at the nanoscale, such as designing micro/nano-devices [87], creating nanostructured materials with optimized mechanical properties [88] and understanding the molecular origins of friction and adhesion [89–91].

3. Main techniques for studying nanoparticles

The research methods frequently used in studying the mechanical properties of nanoparticles will be briefly introduced as follows:

3.1. AFM techniques

AFM is a powerful technique that can be used to obtain both high-resolution images on many kinds of solid surfaces and the vertical force as well as lateral force between a sharp tip and the surface [92–94]. The schematic diagram of the basic working principle of AFM is shown in figure 5, including a cantilever with a sharp tip on its end, piezotube scanner, scanning and feedback systems, a four quadrant photoelectric detector and the computer. Briefly, the sharp tip scans over the sample and the deflection of the cantilever is quantified through a laser beam reflected off the backside of the cantilever and received by the photoelectric detector. If a constant force is kept between the tip and sample during scanning, the topographic image of the sample surface can be obtained by plotting the height of a sample stage on the piezoscanner, which is controlled by a feedback system. Alternatively, the interaction force between the tip and sample can be obtained with the cantilever's vertical deflection using the force-versus-distance curves, briefly called force curves, together with Hooke's law [95, 96]. These curves can provide valuable information on some of the important properties of nanoparticles, such as hardness, elastic modulus and the adhesion between nanoparticle and substrate. The lateral force is closely related to the torsional deflection of the cantilever; an accurate value can be obtained after careful calibration of the cantilever's torsional coefficient [97]. More details about the basics of AFM can be seen in [93, 96].

3.2. Particle tracking velocimetry (PTV)

PTV is an image-based velocimetry method of measuring the velocity field and tracking individual particles in fluidic systems [98, 99]. Fluorescent particles are usually used as tracers within a defined area where those particles are illuminated; then pictures of these particles are taken. The motion trajectories of the particles can be reconstructed by locating them in those pictures and the velocities of the particles can be calculated correspondingly. Based on these, deep insight into some of the complex and low-velocity flows in a region can be acquired. It is a technique that is slightly different from particle image velocimetry (PIV) where the particles' displacements within a segment of an image are averaged [100]. Currently, there are mainly two different PTV methods, i.e. two-dimensional particle tracking velocimetry (2D-PTV) [101] and three-dimensional particle

tracking velocimetry (3D-PTV) [102]. The defined area is a thin light sheet for 2D-PTV while it is an illuminated volume for 3D-PTV, which is usually based on a multiple-camera-system.

3.3. *In situ* TEM

TEM could provide images with a significantly higher resolution than a light microscope by using electrons as 'light source' which have a much lower wavelength [103, 104]. The basic principle is that a beam of electrons passes through a very thin sample and, after interacting with the atoms in the sample, some unscattered electrons reach a fluorescent screen to form an image. The image is shown in varied darkness indicating the material density in different parts of the specimen. The image is magnified and can be studied directly from the screen or recorded with a camera for post-analysis. *In situ* TEM offers the capability of real-time observation of the responses of the microstructural evolution of nanostructures to external active stimuli and their relationship with properties [19, 105]. Active stimuli applied to the sample examined in the microscope during simultaneous imaging include mechanical [19], thermal [106] and electrical [107] ones, etc.

3.4. MD simulation

Computational simulations are usually considered as very useful complementary tools to experimental studies on the mechanical properties of nanoparticles [108]. Among many different kinds of computation methods, MD simulation is an important aspect which could model the time evolution of the physical motions of interacting atoms or molecules [109, 110]. It is a computation method that is based on statistical mechanics; statistical ensemble averages are normally hypothesized to be equal to the time averages of the system. Mostly, in MD simulation, Newton's equations of motion for the atoms or molecules in a system are numerically solved to get their positions and velocities and finally to describe the thermodynamic behaviours of the system. The interactions and potential energy between atoms or molecules are defined by a molecular mechanics force field.

4. Basic mechanical properties of nanoparticles

4.1. Hardness and elastic modulus of nanoparticles

Understanding some basic mechanical properties of nanoparticles, such as the hardness and the elastic modulus, will aid a lot in the proper design of particles in specific applications, as well as evaluating their roles and action mechanisms. To the authors' knowledge, the measurement of the mechanical properties of microparticles has been developed for decades. The microindentation technique was used by Steinitz in 1943 to test the hardness of microparticles with indented areas of larger than 100 μm^2 and a minimum indenter size of 20 μm^2 [111]. About ten years ago, nanoindentation was employed by Shorey *et al* to measure the elastic properties of particles (average size: 5 μm) used for magnetorheological finishing [112].

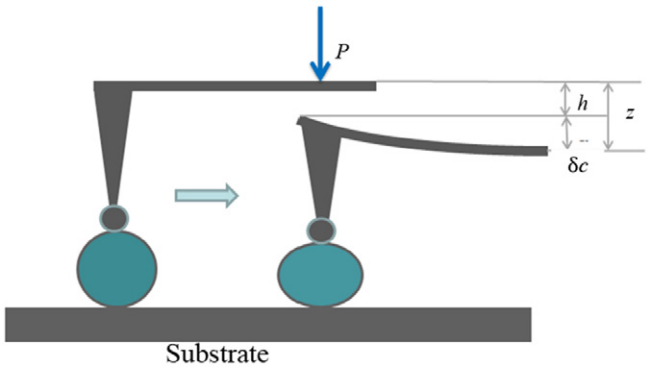

Figure 6. Relative displacements and deformations of the particle-AFM tip system during the indentation process. Left: the AFM tip just touches the particle without deformation of the particle. Right: the particles' deformation occurs due to the applied force by the AFM tip.

Their methods were aimed at measuring the film of particles rather than individual particles. The deformation behaviours of polystyrene microspheres (diameter: 20 μm) by using AFM against a mica surface was firstly investigated by Biggs and Spinks in 1998 [82]. Since then, protocols of calculating the mechanical characteristics (e.g., the elastic modulus) of nanoparticles have developed rapidly, primarily by measuring the particles' deformation with AFM. Typically, quantitative computation of the elastic modulus of nanoparticles requires the measurement of indentation h by converting AFM force-displacement curves into force-indentation curves instead of measuring the contact area radius [21]. The latter is hard to obtain directly. The external load P applied through the cantilever (its spring constant denoted as k) to the tip can be described with the Hooke law,

$$P = k \cdot \delta_c \tag{1}$$

where δ_c is the cantilever deformation. The indentation depth h of the tip into the sample surface is:

$$h = z - \delta_c \tag{2}$$

where z is the piezo displacement. The relative displacements and deformations of the particle-AFM tip system in the indentation process are shown in figure 6. Since there is often system thermal drift, the deflection offset, δ_{c0} should be considered. In this case, equation (1) can be rewritten as

$$P = k \cdot (\delta_c - \delta_{c0}). \tag{3}$$

Also, if the position for the tip initially touching the sample surface is considered, resulting in another height offset z_0, equation (2) becomes

$$h = (z - z_0) - (\delta_c - \delta_{c0}). \tag{4}$$

In this way, the force–indentation curves can be obtained for the calculation of the particles' elastic modulus by evaluating the slope of the loading region on the curves with contact theories. More details about the calculation of the elastic modulus of compressed nanoparticles can be seen in [22, 83, 113].

Table 3. Summary of the hardness and elastic modulus of different particles with the size of several hundreds of nanometres or smaller.

Particle material		Diameter/size	Hardness/(bulk value)	Elastic modulus/(bulk value)	Indentation depth	Notes
Organic nanospheres	Polystyrene(PS) [21, 114]	58–194 nm [21];		8.0–4.1 GPa [21];	3–6 nm [21]	Modulus increases with the decrease of particle size [21]
		180–250 nm [114]		1–2 GPa [114] /(3–3.6 GPa) [115]	5–6 nm [114]	Vinylbenzyl(trimethyl) ammonium chloride units inside [114]
	Polypropylene(PP) [22]	200–500 nm		1.3–2.8 GPa /(1.5–2 GPa)	1.5 nm	
	Polyesters [116]	2–3 nm		0.1–0.3 GPa		Hyperbranched, molecular weight = 3000–7000
	Polyethylenimine (PEI) [117]	15 nm		5–160 MPa	up to 10 nm	Bigger pressure resulted in larger modulus
	Poly-(methylmethacrylate) (PMMA) [118]	350 nm		4.3 GPa/(4 GPa) [115]	up to 60 nm	6.6 GPa (200 °C heat treatment)
	Liquid crystal [119]	95–150 nm		0.1–0.6 GPa	10 nm	4-pentyl-4-cyanobiphenyl (5CB) (main component)
	Core/shell PS/CeO_2 [113]	130–260 nm		5–15 GPa	20–30 nm	Modulus increases with particle size
	PMMA/silica [113, 118]	450 nm [118]; 350 nm [113]		10.3 GPa [118]; 9–11 GPa [113]	up to 80 nm	PMMA-based terpolymer [113]
Metal nanoparticle	Gold [120]	22 nm	1.72 GPa/(Vickers hardness 216 MPa)	100 GPa/(79 GPa)	3–5 nm	Six-fold symmetry gold nanoparticles
	Gold modified with proteins [121]	10 and 20 nm	0.12 and 0.08 GPa [(a)]; 0.22 and 0.13 GPa[(b)]	1.3 GPa[(a)]; 9.5 and 1.0 GPa[(b)]		Protein: (*a*) bovine serum albumin; (*b*) streptavidin pure gold particle: hardness = 0.4 GPa; modulus = 5.2 GPa
	Silver [122]	13 nm	3.12 GPa /(Vickers hardness 251 MPa)	103.9 GPa /(83 GPa)		
Silicon nanoparticle		40–140 nm [123]; 5–40 nm [124]; 40–100 nm [125]	25–34 GPa [124]; 20–50 GPa/ (12 GPa) [125]	600–180 GPa [123]/(around 150 GPa)	13–36 nm [123] 3–24 nm [125]	Modulus increases with decrease of particle size [123]; simulation result [124]
Nanowire, nanotube, etc.	Gold nanowire [126]	40–250 nm		70 ± 11 GPa	400 nm (displacement)	
	Silver nanowire [127, 128]	20–140 nm		75–160 GPa		
	lead nanowire [128]	30–280 nm		14–30 GPa/(16 GPa)		
	ZnO nanowires [129]	70, 99 nm		120, 83 GPa/(140 GPa)		
	WS_2 nanotube [130]	20 nm		171 GPa/(150 GPa [131])		
	Boron nitride (BN) nanotubes [132]	0.58–2.38 nm		40.78–1.85 GPa/(30–40 or 74 GPa)		Single-walled, modulus decreases with diameter increases
	Carbon nanotubes [133]	0.92–1.91 nm		57–9 GPa/(36.5 GPa, bulk graphite [134])		
	Carbon nanotubes [135]	∼9 nm		∼16 GPa		Multi-walled
	Silicon nitride nanobelts [136]	20–50 nm (thickness)		570 GPa (bending modulus) /(120–330 GPa)	150 nm (displacement)	
	Cellulose nanocrystals [137]	4.2 nm (wood), 5.9 nm (cotton) [137] 8–20 nm [138]		24.8, 17.7 GPa [137]; 8.1 GPa(mean value) [138]		Cellulose nanocrystals are crystalline, rod-like shaped particles

Mostly based on the previous method, the elastic modulus of a variety of nanoparticles have been measured by compressing or bending particles primarily with AFM, as summarized in table 3; the hardness of some nanoparticles is also given. As shown, the nanoparticles' hardness and elastic modulus often deviate from their bulk materials' and some show obvious size-dependent behaviours. Typical related results and the underlying mechanisms can be divided as the following three categories.

(1) In the case of spherical polymer nanoparticles, there are yet no uniform size-dependent behaviours of the

mechanical properties. For instance, the compressive moduli of the polystyrene nanoparticles (diameter: 200 nm) were found to be slightly less than those of the corresponding bulk materials due to the presence of hydrated ionic functional groups [21]. In contrast, the work conducted by Paik *et al* [22] showed that the elastic modulus of polypropylene (PP) nanoparticles was higher than that of the bulk material. It was thought that the glass transition temperature (T_g), the crystalline phase and crystallinity etc could affect the deformation of the polymer chain inside and thereby result in the change of the particle's elastic modulus.

(2) For crystalline metal nanoparticles, dislocations inside the particles have been demonstrated as one of the factors contributing to the change in the mechanical behaviour of nanoparticles, which is in contrast to the traditional view that no dislocation is present in crystalline nanoparticles. The experimental work done by Ramos *et al* [120] indicated that the hardness and elastic modulus of six-fold symmetry gold nanoparticles were higher than the bulk phase due to the formation of stacking faults and dislocations in specific crystallographic directions. Mordehai and Nix *et al* [139, 140] performed nanoindentation and compression tests combined with theoretical simulation to reveal the deformation behaviours of single-crystal gold nanoparticles on sapphire substrates. The particle strength under indentation increased with the lateral dimension of the particle due to the competition between the generation of dislocations beneath the indenter and their drainage from the particle [139]. Under compression with a flat diamond punch, the compressive stress of the particle increased with the decrease of the particle size since the nucleated dislocations resulted in the stress gradient along the slip planes [140]. *In situ* TEM nanoindentation experiments showed the direct evidence of the presence of dislocations in metal nanoparticles during deformation but they disappeared during the unloading process, as shown in figure 7 [105]. Wang *et al* [141] recently demonstrated a new kind of stacking fault related with dislocations in gold nanocrystals, which could nucleate, migrate and annihilate under mechanical loading with *in situ* TEM and MD simulation.

For silicon nanoparticles, similar behaviours were observed by Gerberich *et al* [125] that their hardness (particle diameter: 40 nm) was four times greater than the value of bulk silicon. They proposed that the dislocations or line defects inside the particle are the main factors resisting high pressures. Furthermore, atomistic simulation conducted by Zhang *et al* [124] confirmed that the superhard silicon nanoparticles resulted from the nucleation and movement of dislocations. Apart from dislocations or defects, the changes of the lattice strain and the bond energies of nanoparticles to the compressive stress were proposed as another cause for the strengthening and weakening of the mechanical properties of nanoparticles [142]. Furthermore, first-principles electronic-structure calculations made by Cherian *et al* [143] suggested the size dependence of the bulk moduli of several semiconductor nanoclusters correlated with the strong interaction with the passivant.

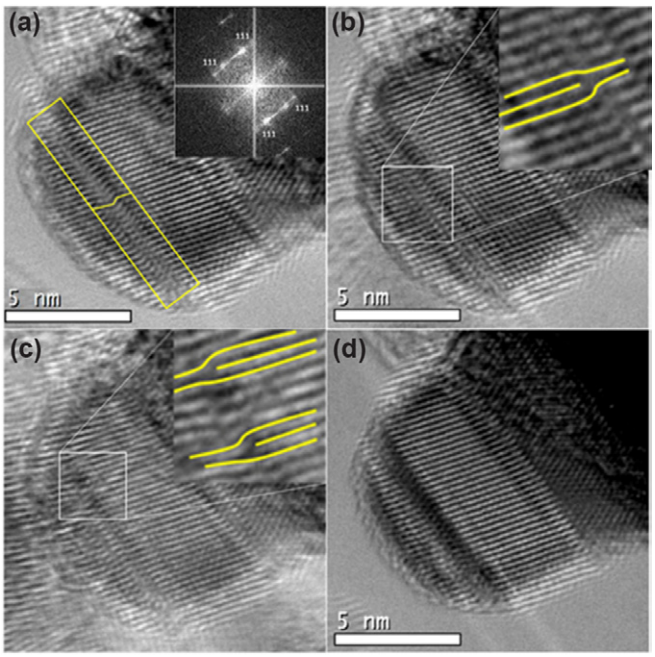

Figure 7. High-resolution TEM images of a silver nanoparticle before and after compression: (*a*) before compression (twin highlighted); (*b*) at the initial stage of compression (an edge dislocation highlighted); (*c*) at a stage of further compression (two additional dislocations shown in the inset); (*d*) after the removal of the compression (no dislocation observed) [105].

(3) For nanowires or nanotubes, it has been typically found by Jing *et al* [127] and Cuenot *et al* [128] that the elastic moduli of silver and lead nanowires decreased with the increasing radial diameter. They proposed that the increase in the modulus was attributed to the effects of the surface stress, the oxidation layer and the surface roughness [127], or the surface tension effect [128]. MD simulations conducted by Yang *et al* [144] showed the bulk modulus of Ni/Ni_3Al nanowires increased but the surface energy decreased with the increasing wire perimeter size. However, only the fracture properties rather than the elastic behaviour of ZnO nanowires were affected by the surface effects due to the presence of surface cracks and defects [129].

Worth mentioning is the fact that measuring the mechanical properties of individual nanoparticles is very complex; many influencing factors could affect the finally measured results. These factors include the uniform dispersion of nanoparticles on an ideally hard substrate, the precise locating of particles and the proper application of loads onto the particles, as well as the measurement of the minimum particle deformation, etc. In addition, many uncertainties during measuring and calculating the mechanical properties of nanoparticles with AFM, e.g., uncertainties associated with the instrument calibration and the calculation models, should be considered [138].

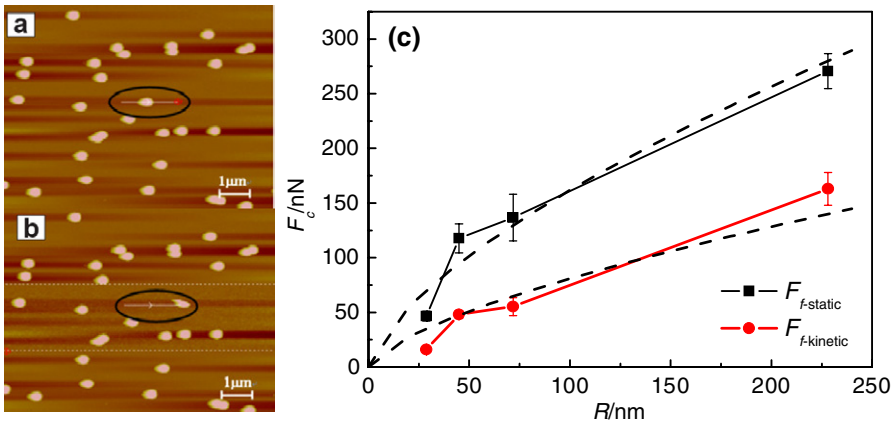

Figure 8. AFM images of a nanoparticle on the substrate (*a*) before and (*b*) after manipulation; (*c*) the dependence of the friction force of polystyrene particles on the silicon surface on the particle radius (R) [24].

4.2. Adhesion and friction of nanoparticles

The adhesion and the friction of nanoparticles play important roles in nanofabrication, lubrication, the design of micro/nano devices, colloidal stabilization and drug delivery. In this case, characterizing the adhesion and friction behaviours of nanoparticles has attracted significant research interest over the past decade [84, 145–157]. So far, AFM has been proved to be a powerful tool to measure the adhesion and friction between a nanoparticle and a solid surface. The AFM tip itself can also be thought of as a nanoparticle; then the adhesion force as well as the friction force can be easily obtained by the cantilever's deflection [151, 154]. However, the use of AFM is practically limited by the tip material and its geometric shape. By attaching the particle to the force sensor in the microscope, the force between a surface and a colloid particle was directly measured with AFM by Ducker *et al* in 1991 [70]. Since the properties of the attached particle, such as the size, the shape and the material were controllable, the uncertainties in the force measurement caused by the irregular shape of the AFM tip etc could be avoided. Hence, the colloidal probe technique is more effective for studying the adhesion and friction of micro/nanoparticles [96, 158]. Nevertheless, it is actually very difficult to attach a single nanoparticle with the size of less than 1 μm on the AFM force sensor; the colloid probes in most references have sizes larger than 1 μm [158]. A chemical method was used by Vakarelski *et al* to place individual gold nanoparticles (20–40 nm) on the tip of an AFM cantilever to measure the adhesion force between nanoparticles and mica [159]. Ceria nanoparticles (50 nm in diameter) were attached on the AFM tip with epoxy glue by Ong and Sokolov [160] to measure the adhesion force between nanoparticles and a flat silica surface. Other various methods include measuring the adhesion force of the tip against a film of nanoparticles [153, 161–163] and manufacturing a tip with a certain curvature by thermal oxidation, etc [164, 165].

Besides the direct adhesion measurement by the vertical deflection of the AFM cantilever, nanoparticle movement manipulation by the cantilever's torsional deflection was firstly used to push C_{60} islands grown on a NaCl surface in 1994 [156]. Since then, this method has been increasingly popular to characterize the intriguing nanoadhesion/friction behaviours of nanoparticles [91]. For instance, the frictional anisotropies for molybdenum oxide (MoO) nanoparticles were investigated by Sheehan and Lieber [166]. The maximum sliding friction force between polymer latex spheres (radius between 50 and 100 nm) and a highly oriented pyrolytic graphite (HOPG) surface was obtained by Ritter *et al* [23]. More recently, the interfacial friction between antimony (Sb) nanoparticles and a HOPG surface was successfully measured through pushing nanoparticles with the AFM tip by Dietzel *et al* [167]. In addition, the adhesion forces between nanoparticles with different sizes and the surface were measured by Guo *et al* [24].

In the most general case, the adhesion force is a combination of electrostatic force, vdW force, meniscus or capillary force, solvation force and structure force, etc. The adhesive contact between elastic surfaces is usually described by single-asperity theories such as JKR, DMT or M-D (Maugis-Dugdale) theories, as mentioned previously. The adhesion force of micro/nanoparticles has been extensively studied and most of the equations for the continuum contact theories can be applied extremely well, even at the submicron scale [82, 85, 168–170]. A linear dependence of the adhesion force on the reduced radius was found by Heim *et al* [170] for the adhesion between silica spheres, proving that the DMT theory was also valid for the particle with dimensions below 1 μm. The simulation of the adhesion between a nickel AFM tip and a gold surface by Landman *et al* [168] showed good agreements with the JKR theory for both the mean positions of atoms and the stress distribution. Individual nanoparticles with varying size from about 50 to 500 nm were manipulated on a silicon surface using AFM by Guo *et al* [24]. The results showed that the friction forces between the particles and the substrate were proportional to the two third power of the radius, which was in agreement with the Hertzian theory, as shown in figure 8. The situations where the continuum contact theories are no longer applicable involve changing surface energy with time [171–173], viscoelastic materials [174, 175] and rough surfaces [176, 177]. All of these factors could give rise to hysteresis and time-dependent effects.

Under ambient conditions, the capillary force (meniscus force) was demonstrated to make the largest contribution to the adhesive force [178]. The capillary force between a plate and a

sphere was calculated by O'Brien and Hermann [179], proving the meniscus dimension was of 1 nm [180, 181]. The adhesion between particles in aqueous media was found to be mainly influenced by the electrostatic force [182, 183], solvent force and structure force [184–186]. For small particles of nanoscale size, more subtle effects beyond continuum theories have been observed. Specifically, the surface molecular structure, the distribution of terminal groups on the particles' surfaces and the surface energy variation due to particle deformation could influence and even dominate the adhesion behaviours [84, 153, 158, 187, 188].

In Amontons and Coulomb's friction theories for describing macroscopic dry sliding friction, the friction is proportional to the normal force, but independent of the contact area as well as the sliding velocity. However, the tribological properties at the micro/nano scale cannot be explained with these empirical theories. Ever since 1987 when the frictional forces were detected with AFM by Mate *et al* [154] for the first time, the friction at the micro/nano scale has been observed by many researchers to deviate considerably from the predictions based on established macroscopic laws. The nanoscopic friction is proportional to the true contact area, which is not necessarily proportional to the loading force [189–191]. Furthermore, the friction in a nanoscale contact increases logarithmically with the sliding velocity [192], being in sharp contrast to empirical theories. The friction between the AFM tip and the substrate has been measured as a function of many parameters, such as the externally applied load [189–191, 193, 194], the sliding velocity [192, 195, 196], the tip radius and shape [189, 191], the relative orientation between the scan direction and the substrate lattice [197–200], the temperature [201, 202] and the chemical nature of the sample [203–205]. The method using the AFM tip to control the lateral manipulation of nanoparticles provides a powerful tool to measure the interfacial friction of nanoparticles with arbitrary materials and sizes. Polymer latex spheres (50–100 nm in radius) were manufactured by Ritter *et al* [23] on a HOPG surface; the threshold force needed to overcome the static friction of a single latex sphere was found to depend on the sphere size, being in accordance with the JKR and DMT theories. Similarly, Sb nanoparticles on a HOPG surface were pushed by Dietzel *et al* [157] with an AFM tip and two coexisting frictional states were observed: some particles showed finite friction and increased linearly with the interfacial areas, while other particles experienced a state of frictionless sliding. The transition from static to kinetic friction was also investigated in another of their work and a hysteretic character in the force domain was found [167]. Polystyrene nanospheres with radii varying from about 30 to 200 nm on the polished nanosmooth silicon surface were manipulated by Guo *et al* [24] with the contact mode of AFM; the typical results are shown in figure 9. The results indicated that the ratios between the kinetic friction $F_{f\text{-kinetic}}$ and the static friction force $F_{f\text{-kinetic}}$ were in the range of 0.3–0.6. Moreover, the ratio did not change whether the particles were located in different areas of the surface, the tip normal force was varied or even the surface was modified [24].

Gold particles with a mean diameter of 25 nm were manufactured by Mougin *et al* [206] on silicon substrates; it

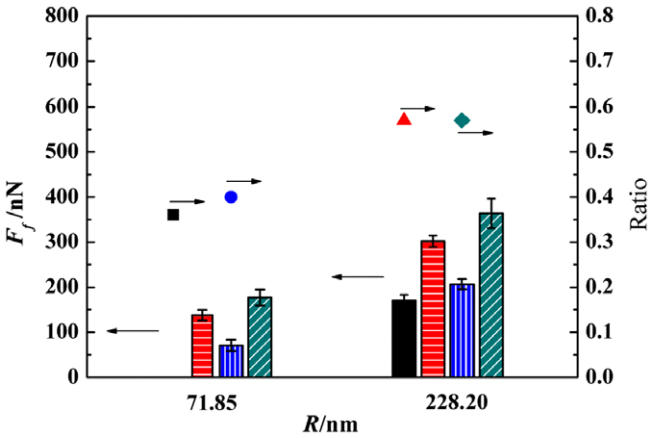

Figure 9. Static and kinetic frictions and their ratios for particles with radii of 71.85 nm and 228.2 nm on a non-hydroxylated surface and a hydroxylated surface, respectively. The normal load is 348 nN. The columns with solid fill and horizontal stripes represent $F_{f\text{-kinetic}}$ and $F_{f\text{-kinetic}}$ on the non-hydroxylated surface, respectively. The columns with vertical and oblique stripes repesent those on the hydroxylated surface, respectively. The square and the circle represent the ratio of $F_{f\text{-kinetic}}$ and $F_{f\text{-kinetic}}$ for particles with R of 71.85 nm on the non-hydroxylated and the hydroxylated surface, respectively. The triangle and the rhombus represent those for particles with ($R = 228.20$ nm) on the non-hydroxylated surface and the hydroxylated surface, respectively [24].

was found that the adhesion of the particles to the substrate was strongly reduced by the presence of hydrophobic interfaces. The friction and wear of spherical gold nanoparticles under dry conditions and submerged in water were studied by Maharaj and Bhushan [207]; the results indicated that the addition of gold nanoparticles reduced friction and wear. Sitti and Hashimoto [208, 209] proposed an AFM-based force-controlled pushing system for the manipulation and assembly of nanoparticles. Interaction forces among the AFM probe tip, the nanoparticle and the substrate, including the vdW force, capillary force, electrostatic force, repulsive contact force and frictional force were analysed [208]; several modes of particle motion including sliding, rolling and rotation were observed [209].

4.3. Movement of nanoparticles

Various forces such as gravitational (buoyancy) forces, surface forces, viscous flow forces and the forces due to Brownian motion result in the movement of nanoparticles in the media in different ways [210–220]. However, the experiments for the direct observation of nanoparticles' movement are limited primarily due to the small particle size preventing the application of the most commonly used imaging techniques. Fortunately, the rapid development of measurement technology provides opportunities for tracking individual nanoparticles or even single molecules. Up to now, several methods have been used for making high-resolution measurements of the motion of single nanoparticles. Among these methods, two groups can be classified: one is to passively track the particle motion without applying significant external stimuli and the other is to measure the particles' motions

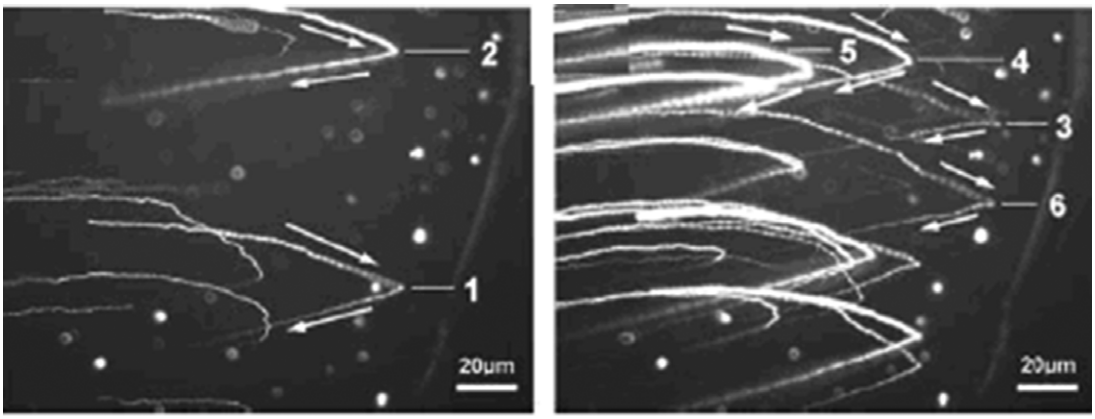

Figure 10. The particle trajectories in a water droplet during the evaporation process [223].

under external mechanical forces [221]. To be more specific, studies based on two typical methods will be emphasized in the following parts.

The first method is particle tracking with the fluorescence technique. A system for observing nanoparticles was developed by Xu *et al* [222] using a high-resolution fluorescence microscope and fluorescent core-shell SiO_2 nanoparticles of 50–60 nm in diameter were used as the seed nanoparticles. By using this system, the velocity profile of nanoparticles in a channel flow [222], the Marangoni flow in evaporating water droplets [223] and nanoparticle–wall collision behaviours [224] were investigated. The Marangoni flow in a droplet manifested with fluorescent nanoparticles revealed a stagnation point where the directions of the surface flow, the surface tension gradient and the surface temperature gradient changed, as shown in figure 10 [223]. The nanoparticle–wall collision experiments showed the nanoparticles adsorbed on the solid surface after collision in liquid were much easier to be removed than those deposited on dry surfaces [224]. The reason for this observation was that the particles might be adsorbed at the secondary minimum of the particle–wall interaction when the collision occurred in water, rather than at the primary minimum for the particles deposited on dry surfaces, as described in the DLVO theory mentioned earlier. Another system for *in situ* observing nanoparticles' movement with the fluorescence technique in confined geometries where external loads and rotations could be applied was developed by Lei *et al* [225]. With this system, it has been found that the velocities of free particles were much larger (20 times) than the rotating speed, providing evidence that nanoparticle impacting was also one of the main surface material removal factors during the surface planarization process. More discussions on this point will be given in the latter part of this review.

The second method is the TEM observations, which could give more delicate details of the particle movement and provide deeper understanding of the roles of particles in specific applications. The movement behaviours of a single MoS_2 nanoparticle in a dynamic contact were directly observed with *in situ* TEM by Lahouij *et al* [226]; the results showed that either a rolling or a sliding process of the fullerenes could be possible during shearing. The motion of inorganic nanoparticles during fluid evaporation was observed using a TEM by Zheng *et al* [227]. The observation of the self-assembled process of nanoparticles in a liquid medium with the particle size comparable to the molecular dimension of the liquid was made using an environmental TEM by Dai *et al* [228].

The movement of nanoparticles is very complicated due to the influence of many factors, e.g., complex forces, medium and environment. In this instance, the studies on the single nanoparticle's motion in the past were mostly qualitative in nature; more precise measurement methods or instruments with a combination of functions are needed for quantitative analyses in future works.

5. Applications relevant to the mechanical properties of nanoparticles

5.1. Nanoparticles in lubrication

The mechanical properties of nanoparticles play a major role in influencing the tribological properties of lubricated systems with nanoparticles. The effects of the mechanical properties of nanoparticles as lubricant additives on the tribological properties differ in various materials. The lubricating properties of typical nanoparticle materials are summarized in table 4. From a general point of view, the combined effects of rolling, sliding and the formation of a third body layer and tribofilms are the main reasons for the increased lubricating behaviour after adding nanoparticles [12], as briefly described in the following parts.

(1) The rolling mode of nanoparticles in the lubricated contact area could provide very low friction and wear; however, the occurrence of this effect is strongly dependent upon some properties, e.g., the shape, the size and the concentration of the nanoparticles in the lubricant [246, 250, 253, 254]. Spherically shaped and mechanically stable nanoparticles without significant agglomeration are favourable for their rolling in the contact area between tribopairs [245]. As far as the intrinsic mechanical properties of nanoparticles are concerned, whether the initial spherical shape of the nanoparticles in the contact area can be preserved or

Table 4. Summary of lubrication properties of nanoparticles of different materials as additives.

Material category	Examples	Lubrication mechanism and regime	Favourable aspects	Unfavourable aspects
Metal nanoparticles	Au [229], Ag [229, 230] Cu [231–233], Ni [234]	(1) Formation of soft and low shear strength tribofilms	Friction and wear reduction, anti-contact fatigue, good extreme pressure	Low dispersibility in organic solvent
	CuO, ZnO and ZrO_2 [235–237], TiO_2 [238] Al_2O_3 [239, 240]	(2) Formation of the third body layer due to mechanical compaction		
	Organically coated modification [233, 241, 242]	(3) Extreme pressure related to the size and the hardness of nanoparticles	More stable colloid system	Modification with chlorine and phosphorus containing compounds are not green
	Metallic-organic complexes [243]	(4) Effective in mixed lubrication and low-load boundary lubrication	Efficient delivery of particles to the asperity contact	
Dichalcogenide MX_2(M = W, Mo; X = S, Se) nanoparticle	WS_2 [244–246], MoS_2 [226, 247, 248], WSe_2 [249]	(1) Rolling/sliding at the low normal stress and exfoliation at the high normal stress under boundary lubrication (2) Layers in the particles can easily slide due to weak intermolecular interactions	Reducing sliding friction, by up to 50%, in the mixed lubrication regime	
Carbon-based nanoparticle	Diamond nanoparticle [218, 250–252]	(1) Ball-bearing effect (2) Viscosity-increasing effect (3) Increase in the surface hardness of tribopair	Friction reduction, anti-scuffing, surface polishing	
	Graphite nanoparticle [253, 254]	Ball-bearing spacers, reduce metal contact and increase the wettability of lubricant on surface	High temperature resistance, extreme pressure and self-lubrication ability	Water insoluble due to hydrophobicity
	Fullerene [255–257]	Similar to dichalcogenide MX_2	More effective for low viscosity base oil and high normal loads	
Silicon nanoparticle	SiO_2 [258–261], Al_2O_3/SiO_2 composite nanoparticles [262]	Bear load, separate tribopair, prevent direct contact, and promote rolling, inhibit the expansion of the microcracks on the tribopair surface due to particle embedment	Cheap and easily available	
Polymer nanoparticle	PTFE nanoparticle [263, 264]	(1) Increased load bearing properties due to large adhesion between lubricant and tribosurface (2) Mechanical energy adsorbed by particles as its deformation occurs (shock-absorbing effect)	Reduce friction and wear; extreme pressure	Unstable under high temperature

not have a close relationship with their hardness/elastic properties, which are also affected by the nanoparticle size [226].

(2) The sliding mode of nanoparticles could also result in low friction and wear. Sliding friction usually occurs when the particle is not very spherical in shape and has low adhesion to the tribopair surfaces [265]. Besides, particle agglomeration in the contact area is another factor that could lead to sliding friction during the shearing of tribopairs [229–233]. In this case, the nanoparticles play a role as a spacer in minimizing the direct contact between the asperities of two shearing surfaces.

Externally applied pressure on the nanoparticles, the rigidity of the tribopair surfaces and the interaction forces between particles are very relevant to the above two modes of particle movement in the lubricated contact area. A smaller applied load and harder tribopair surfaces readily lead to rolling friction of nanoparticles in the contact area, because these would give less of a probability for the particles to mechanically deform or indent into the surface [14, 245]. Moreover, particle agglomeration is greatly determined by the interaction force between particles, thereby inhibiting rolling while promoting the sliding of nanoparticles in the contact area [229, 231]. Another important aspect of the nanoparticle in the lubricant under a low applied pressure is that the viscosity of the lubricant could be enhanced and thereby the oil film formation properties in the lubricated contact could

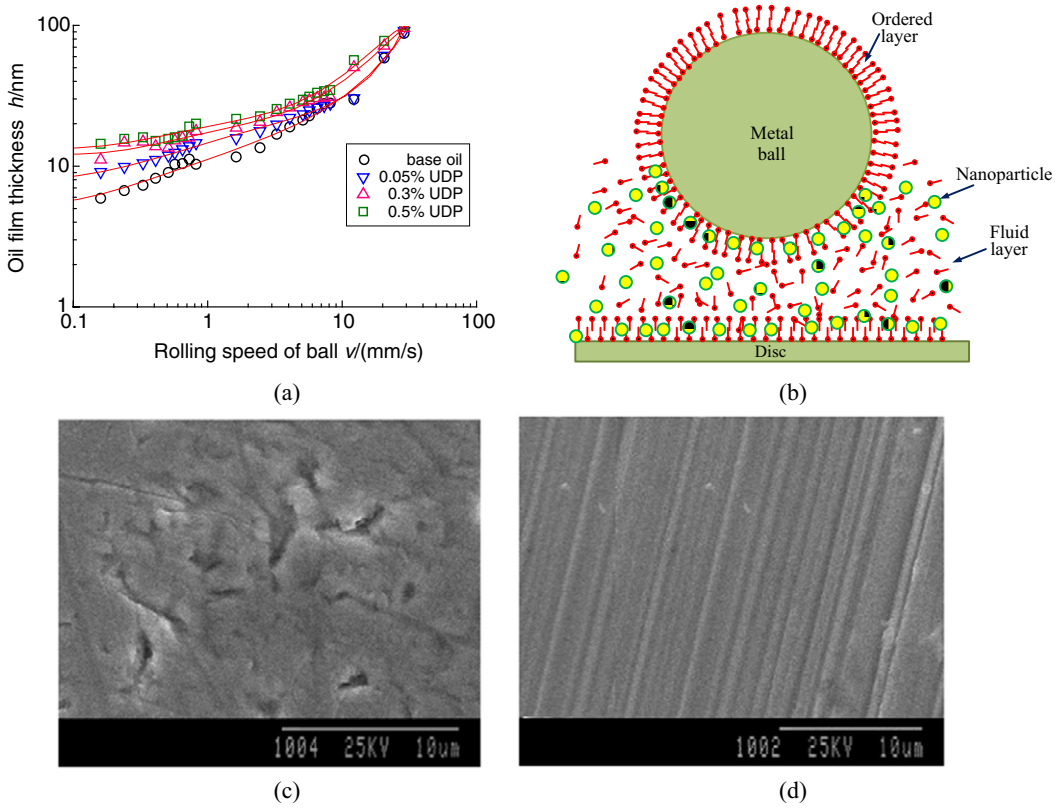

Figure 11. Typical results of lubrication properties of oils (polyester (PE)) with added diamond nanoparticles: (*a*) film thickness against ball rolling speed for PE with nanoparticles of different concentrations (applied pressure: 174 MPa); (*b*) physical model of nanoparticles as additive; (*c*) SEM image of the rubbing surface under PE lubrication (rubbing time: 30 min; applied pressure: 220 MPa); (*d*) SEM image of the rubbing surface under PE lubrication with nanoparticles (rubbing time: 30 min; applied pressure: 220 MPa) [218].

be improved, as shown in figures 11(*a*) and (*c*) [218]. It can also be noted from this figure that when the applied pressure increased further, the sliding effect of nanoparticles could give rise to the surface polishing effect.

(3) When the applied pressure is sufficiently large, nanoparticles become mechanically unstable and delamination of nanoparticles could happen [245, 246]. For instance, studies suggested that when the applied pressure was ∼1 GPa and the tribopair operated in the boundary lubrication regime, exfoliation of inorganic fullerene-like (IF) nanoparticles as the lubricant additive would dominate [244–247]. In this case, material layers of the broken particles could form as the third body and adhere on the tribopair surfaces separating the counterpart. These layers likely align themselves parallel to the tribopair surfaces due to adhesion and shear. It occurs more often for metal dichalcogenide and graphite nanoparticles, which have anisotropic layered structures with weak vdW forces as the bonding interaction between layers [226, 244–249, 253–257]. In addition, valleys between asperities could be filled out by nanoparticles; then the tribopair surface could be partly smoothened out to reduce friction and wear [261].

It is worth pointing out that nanoparticles as lubricant additives do not always give rise to favourable tribological properties. Increases in friction and wear, as well as lubricant starvation, were observed due to the abrasive effect of hard nanoparticles under large pressures and heavy aggregations of oils with high particle concentrations in the inlet of the contact area [264].

5.2. Nanoparticles in nanomanufacturing

As already mentioned in the introduction, CMP is an indispensable planarization tool in nanomanufacturing ICs. Abrasive and corrosive slurry is used to physically grind and chemically remove microscopic topographic features on a wafer to obtain a flat surface [215]. In this process, abrasive nanoparticles in the slurry are a very important contributor to obtain controlled material removal without sacrificing planarity. They usually either embed in the polishing pad or remain immersed in the slurry, as schematically shown in figure 12 [265]. Among many factors that could affect the material removal rate and surface quality in CMP, the mechanical interaction between the nanoparticles and the wafer surface plays a critical role. For the material removal process, two models have been proposed to understand the mechanical behaviours of abrasive nanoparticles in CMP, i.e. the hydrodynamic model and the solid contact model [266, 267].

(1) In the hydrodynamic model, the wafer and the polishing pad are separated by a thin liquid film; the material removal is primarily due to the collision of abrasive nanoparticles onto the wafer, or the fluidic shearing.

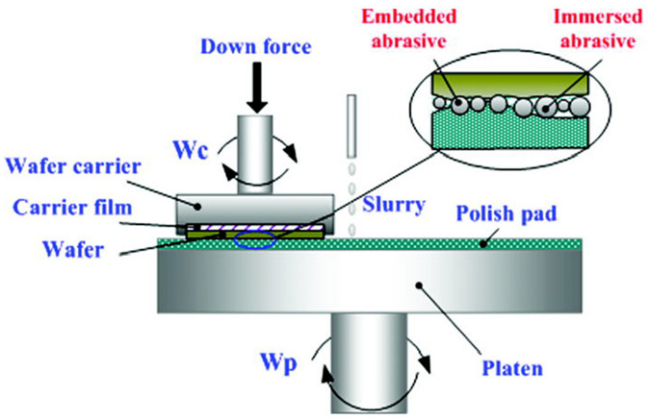

Figure 12. Schematic illustration of the CMP tool and the contact among wafer, pad asperity and abrasive particles during the CMP process [265].

The effects of the particle size, the incidence speed and angles etc on the collision between nanoparticles and the wafer surface have been investigated [214, 224, 268, 269]. Xu *et al* [224] designed an experiment based on a fluorescent microscope system where fluorescent nanoparticles adsorbed on a glass surface were exposed to the vertical impact of a liquid with 15 wt% abrasive nanoparticles. The results suggested that the collision between the abrasives and the wafer surface had a negligible effect on the material removal at a liquid impact speed of $3\,\mathrm{m\,s^{-1}}$. When the impacting speed was increased and the nanoparticle incidence angle was changed, damage to the wafer surface could occur. For instance, there were many pits and scratches on the surface on the wafer surface under a speed of $50\,\mathrm{m\,s^{-1}}$ and an incidence angle of 45°; heavy and heterogeneous deformation in the surface layer was observed with the high-resolution TEM [214], as shown in figure 13. MD simulation studies on the collision process of a nanoparticle onto a silicon or silica surface suggested the damage could be increasingly reduced with the increasing incident angle [269–271]. Moreover, the critical velocity for the pileup formation on the silicon surface is affected by the incidence angle rather than the particle size [270].

(2) In the solid contact model, part of the polishing pad is in direct contact with the wafer surface [272, 273]. The particles embedded in the pad slide against the substrate surface, in a similar way to fixed abrasive grinding (referred to as fixed particles). The particles immersed in the slurry between the pad and the wafer can be referred to as free particles. Lei *et al* [225] used a fluorescence based experimental system to track the movement of individual particles between the polishing pad and the solid surface. The results confirmed that some particles were fixed on the polishing pad and rotated with the pad, while the others moved freely in the slurry flow. Paul *et al* [274] proposed that the ratio of the number of fixed particles and that of free particles was of great importance to the material removal mode. In regard to this model, it has been widely accepted that the material removal is due to the two-body abrasion between the polishing pad and the wafer surface, as well as that between nanoparticles and the wafer surface [266, 267, 275–277]. Nevertheless, increasing evidence shows that the rolling of free nanoparticles in the slurry is not notably inferior to abrasive sliding for the material removal and surface finish on the atomic scale in the CMP process [265, 278]; a typical MD simulation result is shown in figure 14.

Another important aspect is understanding the adhesion and the removal of nanoparticles on the wafer surface; this is a relevant problem in the post-CMP cleaning process [279]. Interfacial forces, such as the vdW force, electrostatic force and capillary force in the vicinity of the nanoparticle and the wafer surface dominate the adhesion process [280]. Many experimental factors could influence the adhesion strength between the particle and the wafer surface, as the following list demonstrates.

(1) The adhesion could increase with the contact time, since the contact area and then the interfacial forces increase as time progresses [281].
(2) Large atmospheric humidity could accelerate the adhesion formation [282].
(3) The size effect of nanoparticles on the adhesion strength has been a research focus and some contradictory results have been obtained. Heim *et al* [170] found that the relationship between microparticle/wafer surface adhesion and the particle radius agreed with the prediction of contact theories. On the contrary, the results obtained by Thoreson *et al* suggested that no size effect of the particle/wafer surface adhesion could be observed [283]. This trend was also confirmed by the experiments conducted by Lei *et al* [225], in which a series of heat-treated AFM probes with various curvature radii were employed to measure the particle/wafer surface adhesion. This result might be as a result of the reduction of the real contact area caused by asperities on the tip surface [284].
(4) In addition, the influence of capillary force should be also considered, since small particles could aggregate to form larger ones [43].

After nanoparticles are adsorbed onto the wafer surface due to the action of interfacial forces, they could be embedded in the surface by pad pressure if valleys or asperities are present on the surface [285]. In this case, the number of residue nanoparticles on the wafer surface after the CMP process could reduce when the wafer surface hardness increases [286]. These residue nanoparticles should be removed during the post-CMP cleaning process to avoid their unfavourable effects on the follow-up processes [287]. Applying external mechanical stimuli, megasonic cleaning as well as some wet chemical effects are optional ways to overcome the adhesion force and remove physisorbed (in some cases chemisorbed) or partially embedded nanoparticles, as schematically shown in figure 15.

The mechanical removal forces are very complex, mainly including the contact elastic force, the hydrodynamic drag force and the friction between a brush and nanoparticles, etc [288, 289]. A schematic description of all the forces

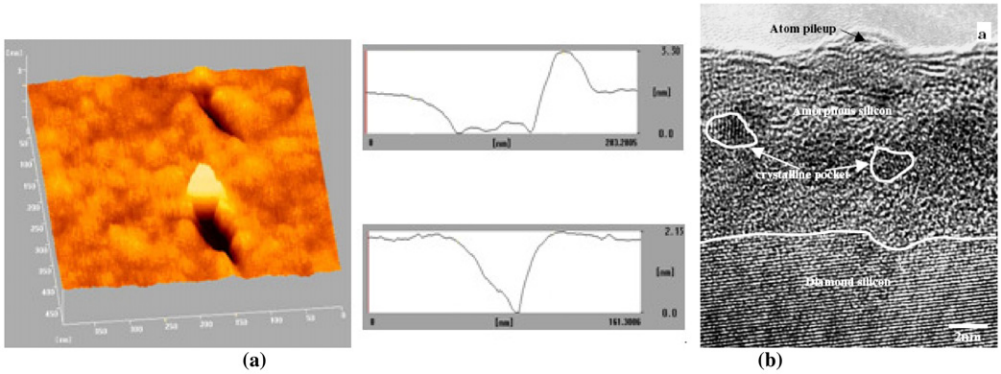

Figure 13. (*a*) AFM image of the surface after a 10 min exposure; (*b*) cross-section high-resolution TEM images of the specimen subsurface after exposure [214].

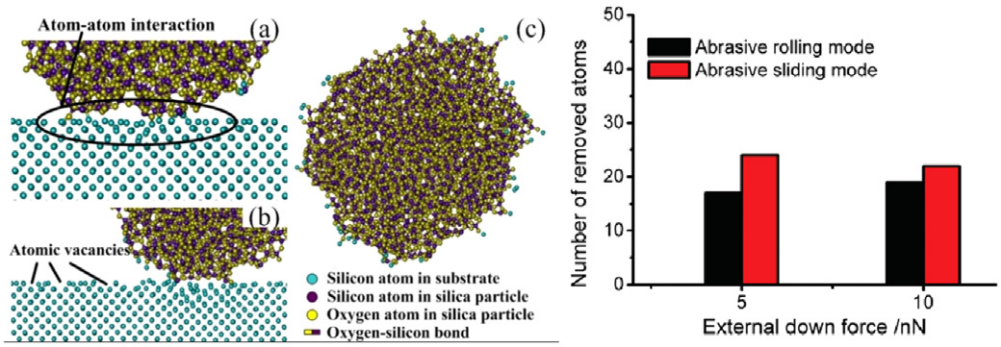

Figure 14. The rolling process of a silica particle under an external down force of 5 nN and a lateral driving force of 10 nN (left); The number of removed atoms against various external down forces with abrasive rolling and abrasive sliding (right) [265].

for a nanoparticle on the surface in the cleaning process was put forward by Huang *et al* [290]. Furthermore, contact models and lubrication hydrodynamic theories were employed to analyse the fluid flow field and calculate the hydrodynamic drag force, as well as the surface roughness and the characteristics of the brush nodules were considered [291].

The mechanical brush scrubbing method is very efficient for removing residue particles; however, it becomes less effective when the particle size is very small, e.g., a nanoparticle. In this case, megasonic cleaning and chemically-activated removal could be adopted. Megasonic cleaning is to utilize a sound field with a frequency of typically 0.8–2 MHz to excite controlled cavitation, which is gentler and on a much smaller scale than that produced under ultrasonic cleaning. Increases in the megasonic frequency, the cleaning period and the solution temperature etc could improve the cleaning effects [292–295]. Nevertheless, this cleaning method has some problems, e.g., the instability of the sound field for cleaning large size wafers and low cleaning efficiency. The basic idea of the chemically-activated removal, i.e. using a chemical additive, is to weaken the bonds between particles [296] or to change the charges on the wafer surface and the particles (alter the solution pH [297, 298] or add surfactants [299]) for controlling the electrostatic repulsion between the particles and the wafer surface.

5.3. Nanoparticles in coatings

Incorporating different kinds of nanoparticles within a metal or polymer matrix to produce nanocomposites can deliver improved properties, such as enhanced mechanical properties, self-lubrication, wear-resistance and energy-absorbing capabilities [300]. A few examples demonstrating the influence of nanoparticles on the mechanical (hardness, elastic modulus as well as tensile strengths etc) and tribological properties of nanocomposite coatings are shown in table 5. There are two main categories of nanocomposites, which are summarized as follows.

(1) Due to some of the inherent properties of the matrix, for instance the high strength and modulus, wear resistance and high thermal and electrical conductivity, metal or metal alloy matrix composite coatings show distinct advantages over polymeric composites [315]. In these coatings, ceramic (Al_2O_3 [301, 304, 306], TiO_2 [305], SiC [307, 308]) and carbon-based (graphite [316] and CNTs [317]) nanoparticles are usually added. There are three reasons why ceramic particles are used as reinforcement to enhance the hardness and the wear-resistance of composites:

- the high hardness and strength of particles [306, 308]
- migration and dislocation motion of grain boundaries can be prevented by the particles in the matrix [304]
- heterogeneous nucleation effect of particles in metal or metal alloys [308].

The addition of graphite nanoparticles or CNTs in a metal matrix could, on the one hand, reduce the porosity of a pure metal coating, then the coating would be much denser and compact with fewer cracks. On the other hand,

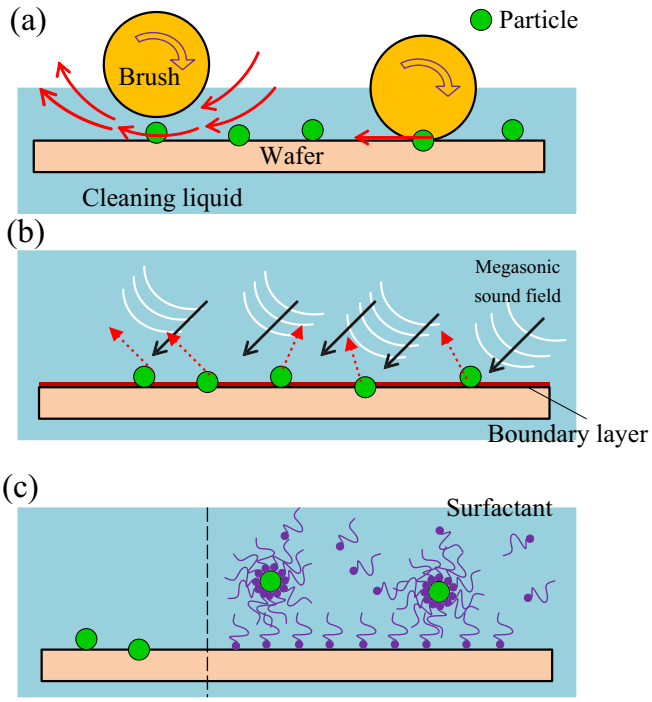

Figure 15. Basic schematic models of typical post-CMP cleaning of nanoparticles: (*a*) brush–particle mechanical interaction; (*b*) megasonic cleaning; (*c*) chemical additive (surfactant).

the crystalline size in the coating could be refined due to the presence of nanoparticles. In addition, the structural and chemical stability of CNTs, which have a higher stiffness and strength compared with the metal matrix are another important factor contributing to the strengthening effect [317].

(2) Modification of the physical properties of a polymer matrix can be achieved by adding inorganic or organic nanoparticles, causing some new characteristics of polymers to be obtained [318]. For example, polymer composite coatings containing some inorganic nanoparticles can provide resistance to the initiation and propagation of cracks, fill cavities and initiate crack bridging, deflection and bowing [319]. Basically, the mechanical properties of polymer based nanocomposites can be affected by many factors, among which the interface between the nanoparticle and the polymer matrix plays a dominant role due to the large specific surface area of the particle [310, 318]. Hence, a good design of a nanocomposite, by taking the complex interplay between matrix, interface and nanoparticles into consideration, could tailor the composite material system with desirable physical properties. Several underlying mechanisms responsible for the interface reinforcement are:

(1) the interaction between nanoparticles and the polymer matrix could result in the formation of special microstructures (for instance, a finer scale lamellar structure), correspondingly the improved mechanical properties could prevent rapid crack propagation in the coating [320];

(2) nanoparticles could enhance their interaction with the matrix through chemical bonds (for example, increase the cross-linking densities in the coatings) or increase the physical interactions between macromolecular chains of the matrix [313, 314, 321]. In this manner, effective pathways could be provided for nanoparticles to complement the poor mechanical and tribological performances of some polymer matrices, e.g., their poor resistance to surface abrasion and wear [319].

Uniform dispersion of nanoparticles in the matrix is very crucial in obtaining improved mechanical properties (e.g., strength and ductility) of nanocomposite coatings, since the maximum filling content of nanoparticles with a large surface area is limited [318]. When the content of nanoparticles in the nanocomposite coatings exceeds a critical value, particle agglomeration would happen, resulting in deterioration of the mechanical properties (for instance, aggravated microcracks on the coating surface), decrease in Young's modulus and increase in the wear rate [313, 319]. In order to achieve good particle dispersion, appropriate preparation and processing methods are needed. Specifically, powder metallurgy and vapour phase processing [315], ultrasonic assisted melting and disintegrated melt deposition, mechanical alloying and friction stir processing [322], as well as layer-by-layer deposition [323, 324] have been used. In addition, the interface between the nanoparticle and the matrix can be modified precisely on the molecular/atomic level with techniques, such as atomic layer deposition (ALD) [325] or molecular assembly to obtain some interesting structures, e.g., core/shell hybrid nanoparticles [326].

6. Conclusion and outlook

Increasingly high requirements of the surface and interface properties of many mechanical systems demand new designs and improvements of surface modifications and manufacturing technologies. Nanoparticles exhibiting many unique mechanical properties have become one of the most attractive choices for meeting these needs in the past couple of years. The foregoing parts review basic physics and recent important results of nanoparticles from the perspectives of their mechanical properties and interfacial interactions, as well as related applications. Available fundamental research data regarding the mechanical properties of nanoparticles provide valuable guidance for their effective implementation in surface engineering, micro/nanomanufacturing and nanofabrication etc. Many of these applications with nanoparticles have already made impressive progress in practice and exhibited significant advantages in many fields.

Despite these, further works are still needed to acquire information on the mechanical properties of more kinds of nanoparticles with the advances of convenient characterization techniques and mature nanoparticle production technologies. Quantitative descriptions of the mechanical properties of nanoparticles in relation to the size dependent and material effects etc should be also made. Additionally, how to achieve a much clearer picture about the roles of nanoparticles in their specific applications is of great significance. Hence, direct

Table 5. Summary of the mechanical properties of some nanocomposite coatings.

	Nanoparticle/matrix	Increased hardness (H) or modulus (M)	Maximum tensile(T) or flexural (F) strength	Friction coefficient (COF)/wear rate(WR)	Optimum particle concentration	Particle size (nm)
Metal matrix	Al_2O_3 [301], AlN [302], MgO [303]/Al or Al alloy	(H)68.4 HRF(115%) [301] (H)1.59 GPa (50%) (M)140 GPa (56%) [302]	(T) 250 MPa (67%) [301] Compressive strength 288 MPa(164%) [303]		4–7 vol% [301, 303] 39 vol% [302]	40–80
	Al_2O_3/Ni-W [304] TiO_2/Ni [305]	(H)8.5 GPa (31%) [304] (H)400 HV (23%) [305]	1460 MPa (1180%), residual stresses [304]	−(50–75)% [303]; −40% (WR) [305]	5–7 wt% [304] 12 g l^{-1} [305]	30–90
	(WC, ZrO_2, Al_2O_3, and Si_3N_4)/(Co or Fe) [306]	(H) increase by 5–16 HRB	bending strength increase by 54%	−(50–90)% (WR), −75% (COF)	2–6 vol%	10–100
	SiC/Mg alloy [307, 308]		(T) 216 MPa(24%); Yield strength 384 MPa(113%) [308]		10 vol% [307] 0.5 wt% [308]	∼20 [307]; 50 [308]
	Nanographite/Cu [309]	(H) 94 HV (31%, 5 vol%)		−23%(COF, 15 vol%), −33%(WR, 15 vol%)		35
Polymer matrix	SiAlON, [310] SiO_2 [311]/Epoxy resin	(H) 67(Shore-D, 18%) [310] (M) 60 MPa (−40%) aggregation, 5 wt.% [311]	(T)18 MPa(-44%) aggregation, 5 wt.% [311]	−67% (WR, 3 wt%) [310]	9–11 wt% [310]	70 [310]
	ZnO/polyurethane [12]		(T) 17.83 MPa (108%)		2 wt%	27
	nano-PTFE/Phenol resins [313]	(H)112 HRM (25.8%)	(F)110 MPa (19.6%)	−33%(COF); −61% (WR)	2–5 wt%	20–80
	PTFE-MoS_2-Al_2O_3/polyoxy-methylene [314]	(H)123 MPa (7%)	(T)52.08 MPa (−7%)		3 wt%	10–30

visualizations of the interfacial behaviour of nanoparticles in applications on the micro-/nano- and even atomic scales would be very helpful.

Acknowledgments

The authors gratefully acknowledge the support of NSFC (Nos 51375255, 51027007 and 51105221), the International Science & Technology Cooperation Project (No 2011DFA70980) and the National Key Basic Research Program of China (Grant No 2011CB013102).

References

[1] Garg A *et al* 2011 Formulation, characterization and application on nanoparticle: a review *Der Pharmacia Sin.* **2** 17–26
[2] Akbari B, Tavandashti M P and Zandrahimi M 2011 Particle size characterization of nanoparticles—a practical approach *Iran. J. Mater. Sci. Eng.* **8** 48–56
[3] Schmid G 2004 *Nanoparticles: From Theory to Application* (Weinheim: Wiley-VCH)
[4] Mohanraj V and Chen Y 2006 Nanoparticles—a review *Trop. J. Pharm. Res.* **5** 561–73
[5] Manmode A S *et al* 2009 Nanoparticles-Tremendous therapeutic potential: a review *Int. J. Pharm.Tech. Res.* **1** 1020–27
[6] Bresme F and Oettel M 2007 Nanoparticles at fluid interfaces *J. Phys.: Condens. Matter* **19** 413101
[7] Garcia M A 2011 Surface plasmons in metallic nanoparticles: fundamentals and applications *J. Phys. D: Appl. Phys.* **44** 283001
[8] Lu A H, Salabas E L and Schuth F 2007 Magnetic nanoparticles: synthesis, protection, functionalization, and application *Angew. Chem. Int. Edn Engl.* **46** 1222–44
[9] Meng X T *et al* 2011 Magnetic CoPt nanoparticles as MRI contrast agent for transplanted neural stem cells detection *Nanoscale* **3** 977–84
[10] Zhang H W, Liu Y and Sun S H 2010 Synthesis and assembly of magnetic nanoparticles for information and energy storage applications *Front. Phys. China* 5 347–56
[11] Luo X L *et al* 2006 Application of nanoparticles in electrochemical sensors and biosensors *Electroanalysis* **18** 319–26
[12] Liu W M and Wang X B 2012 *Nanoparticle-Based Lubricant Additives* (SpringerReference)
[13] Hussain F *et al* 2006 Polymer–matrix nanocomposites, processing, manufacturing, and application: an overview *J. Comput. Mater.* **17** 1511–75
[14] Akbulut M 2011 Nanoparticle-based lubrication systems *J. Powder Metall. Min.* **1** 1

[15] Basmi G B *et al* 2000 Effect of particle size, chemical mechanical poishing slurries for enhanced polishing with minimal defects *J. Electrochem. Soc.* **147** 3523–8

[16] Ilie F 2012 Models of nanoparticles movement, collision, and friction in chemical mechanical polishing *J. Nanopart. Res.* **14** 752

[17] Shin C H *et al* 2009 Single nanoparticle alignment by atomic force microscopy indentation *Appl. Phys. Lett.* **94** 163107

[18] Daeinabi K and Korayem M H 2011 Indentation analysis of nano-particle using nano-contact mechanics models during nano-manipulation based on atomic force microscopy *J. Nanoparticle Res.* **13** 1075–91

[19] Casillas G *et al* 2012 In situ TEM study of mechanical behaviour of twinned nanoparticles *Phil. Mag.* **92** 4437–53

[20] Lahouij I *et al* 2012 Real time TEM imaging of compression and shear of single fullerene-like MoS_2 nanoparticle *Tribol. Lett.* **45** 131–41

[21] Tan S S *et al* 2004 Nanoscale compression of polymer microspheres by atomic force microscopy *Langmuir* **20** 7015–20

[22] Paik P*et al* 2007 Measurement of mechanical properties of polymer nanospheres by atomic force microscopy: effects of particle size *Micro Nano Lett.* **2** 72–7

[23] Ritter C *et al* 2002 Controlled translational manipulation of small latex spheres by dynamic force microscopy *Langmuir* **18** 7798–803

[24] Guo D *et al* 2013 Measurement of the friction between single polystyrene nanospheres and silicon surface using atomic force microscopy *Langmuir* **29** 6920–5

[25] Feynman R P 1959 There's plenty of room at the bottom *Talk in American Physical Society Meeting (Pasadena, CA)* (Pasadena, CA: California Institute of Technology)

[26] Keesom W H 1912 On the deduction of the equation of state from Boltzmann's entropy principle' *KNAW Proc.* **15** 240–56

[27] Debye P 1921 Molecular forces and their electrical interpretation *Phys. Z.* **22** 302–8

[28] London F 1937 The general theory of molecular forces *Trans. Faraday Soc.* **33** 8b-26

[29] Israelachvili J N 2011 *Intermolecular and Surface Forces* 3rd edn (Salt Lake City, UT: Academic)

[30] Derjaguin B V 1934 Friction and adhesion: IV. The theory of adhesion of small particles *Kolloid Z.* **6** 155–64

[31] Hamaker H C 1937 The London–van der Waals attraction between spherical particles *Physica* **4** 1058–72

[32] Dzyaloshinskii I E, Lifshitz E M and Pitaevskii L P 1961 General theory of van der waals' forces *Phys.—Usp.* **4** 153–76

[33] Myers D 1999 *Surfaces, Interfaces, and Colloids* (New York: Wiley-Vch)

[34] Helmholtz H 1853 Ueber einige Gesetze der Vertheilung elektrischer Ströme in körperlichen Leitern mit Anwendung auf die thierisch-elektrischen Versuche *Ann. Phys.* **165** 211–33

[35] Gouy G 1910 Constitution of the electric charge at the surface of an electrolyte *J. Phys.* **9** 457–67

[36] Chapman D L 1913 LI. A contribution to the theory of electrocapillarity *Phil. Mag.* **25** 475–81

[37] Stern O 1924 The theory of the electrolytic double-layer *Z. Elektrochem.* **30** 508–16

[38] http://web.nmsu.edu/~snsm/classes/chem435/Lab14/double_layer.html

[39] Debye P and Hückel E 1923 De la theorie des electrolytes: i. Abaissement du point de congelation et phenomenes associes *Phys. Z.* **24** 185–206

[40] Ruths M and Israelachvili J N 2008 *Surface Forces and Nanorheology of Molecularly Thin Films: Nanotribology And Nanomechanics* (Berlin: Springer) pp 417–515

[41] Haines W B 1925 Studies in the physical properties of soils: II. A note on the cohesion developed by capillary forces in an ideal soil *J. Agric. Sci.* **15** 529–35

[42] Fisher R A 1926 On the capillary forces in an ideal soil; correction of formulae given by WB Haines *J. Agric. Sci.* **16** 492–505

[43] Kralchevsky P A and Denkov N D 2001 Capillary forces and structuring in layers of colloid particles *Curr. Opin. Colloid Interfce Sci.* **6** 383–401

[44] Butt H J and Kappl M 2009 Normal capillary forces *Adv. Colloid Interf. Sci.* **146** 48–60

[45] Denkov N D *et al* 1993 Two-dimensional crystallization *Nature* **361** 26

[46] Kralchevsky P A and Nagayama K 2000 Capillary interactions between particles bound to interfaces, liquid films and biomembranes *Adv. Colloid Interface Sci.* **85** 145–92

[47] Orr F M, Scriven L E and Rivas A P 1975 Pendular rings between solids: meniscus properties and capillary force. *J. Fluid Mech.* **67** 723–42

[48] Visser J 1989 Van der Waals and other cohesive forces affecting powder fluidization *Powder Technol.* **58** 1–10

[49] Richefeu V, El Youssoufi M S and Radjai F 2006 Shear strength properties of wet granular materials *Phys. Rev.* E **73** 051304

[50] Kohonen M M *et al* 2004 On capillary bridges in wet granular materials *Physica* A **339** 7–15

[51] Bowling R A 1989 A theoretical review of particle adhesion *Particles on Surfaces* vol 1 (New York: Springer) pp 129–42

[52] Eve J K *et al* 2002 A study of single drug particle adhesion interactions using atomic force microscopy *Int. J. Pharm.* **238** 17–27

[53] Zhao Y P 2003 Stiction and anti-stiction in MEMS and NEMS *Acta Mech. Sin.* **19** 1–10

[54] Kralchevsky P A and Nagayama K 1994 Capillary forces between colloidal particles *Langmuir* **10** 23–36

[55] Whitesides G M and Grzybowski B 2002 Self-assembly at all scales *Science* **295** 2418–21

[56] Israelachvili J and Gourdon D 2001 Putting liquids under molecular-scale confinement *Science* **292** 867–8

[57] Gerstenberg M C, Pedersen J S and Smith G S 1998 Surface induced ordering of micelles at the solid–liquid interface *Phys. Rev.* E **58** 8028–31

[58] Kocevar K and Musevic I 2003 Structural forces near phase transitions of liquid crystals *Chem. Phys. Chem.* **4** 1049–56

[59] Marcelja S and Radic N 1976 Repulsion of interfaces due to boundary water *Chem. Phys. Lett.* **42** 129–30

[60] Kornyshev A A and Leikin S 1989 Fluctuation theory of hydration forces: The dramatic effects of inhomogeneous boundary conditions *Phys. Rev.* A **40** 6431–7

[61] Leikin S and Kornyshev A A 1991 Mean-field theory of dehydration transitions *Phys. Rev.* A **44** 1156–68

[62] 40.5 Klein J 2013 Hydration lubrication *Friction* **1** 1–23

[63] Derjaguin B and Landau L 1941 Theory of the stability of strongly charged lyophobic sols and of the adhesion of strongly charged particles in solutions of electrolytes *Acta Phys. Chim. URSS* **14** 633

[64] Verwey E J W and Overbeek J Th G 1948*Theory of the Stability of Lyophobic Colloids* (Amsterdam: Elsevier)

[65] Missana T and Adell A 2000 On the applicability of DLVO theory to the prediction of clay colloids stability *J. Colloid Interface Sci.* **230** 150–6

[66] Ninham B W 1999 On progress in forces since the DLVO theory *Adv. Colloid Interface Sci.* **83** 1–17

[67] Hermansson M 1999 The DLVO theory in microbial adhesion *Colloids Surf.* B **14** 105–19

[68] Brant J, Lecoanet H and Wiesner M R 2005 Aggregation and deposition characteristics of fullerene nanoparticles in aqueous systems *J. Nanopart. Res.* **7** 545–53

[69] Hoek E and Agarwal G K 2006 Extended DLVO interactions between spherical particles and rough surfaces *J. Colloid Interface Sci.* **298** 50–8

[70] Ducker W A, Senden T J and Pashley R M 1991 Direct measurement of colloidal forces using an atomic force microscope *Nature* **353** 239–41

[71] Crocker J C and Grier D G 1994 Microscopic measurement of the pair interaction potential of charge-stabilized colloid *Phys. Rev. Lett.* **73** 352–5

[72] Adler J J, Rabinovich Y I and Moudgil B M 2001 Origins of the non-DLVO force between glass surfaces in aqueous solution *J. Colloid Interface Sci.* **237** 249–58

[73] Hertz H 1881 On the contact of elastic solids *J. Reine Angew. Math.* **92** 156–71

[74] Johnson K L, Kendall K and Roberts A D 1971 Surface energy and the contact of elastic solids *Proc. R. Soc. Lond.* A **324** 301–13

[75] Derjaguin, B V, Muller V M and Toporov Y P 1975 Effect of contact deformations on the adhesion of particles *J. Colloid Interface Sci.* **53** 314–25

[76] Tabor D 1977 Surface forces and surface interactions *J. Colloid Interface Sci.* **58** 2–13

[77] Maugis D 1992 Adhesion of spheres, The JKR–DMT transition using a Dugdale model *J. Colloid Interface Sci.* **150** 243–69

[78] Dugdale D 1960 Yielding of steel sheets containing slits *J. Mech. Phys. Solids* **8** 100–4

[79] Greenwood J A 1997 Adhesion of elastic spheres *Proc. R. Soc. Lond.* A **453** 1277–97

[80] Carpick R W, Ogletree D F and Salmeron M 1999 A general equation for fitting contact area and friction versus load measurements *J. Colloid Interface Sci.* **211** 395–400

[81] Maugis D and Pollock H M 1984 Surface forces, deformation and adherence at metal microcontacts *Acta Metall.* **32** 1323–34

[82] Biggs S and Sprinks G 1998 Atomic force microscopy investigation of the adhesion between a single polymer sphere and a flat surface *J. Adhes. Sci. Technol.* **12** 461–78

[83] Armini S, Vakarelski I U and Whelan C M 2007 Nanoscale indentation of polymer and composite polymer-silica core-shell submicrometer particles by atomic force microscopy *Langmuir* **23** 2007–14

[84] Luan B and Robbins M O 2005 The breakdown of continuum models for mechanical contacts *Nature* **435** 929–32

[85] Miesbauer O, Götzinger M and Peukert W 2003 Molecular dynamics simulations of the contact between two NaCl nano-crystals: adhesion, jump to contact and indentation *Nanotechnology* **14** 371

[86] Cheng S and Robbins M O 2010 Defining contact at the atomic scale *Tribol. Lett.* **39** 329–48

[87] Bhushan B 2004 *Handbook of Nanotechnology* (Berlin: Springer)

[88] Valiev R 2002 Nanomaterial advantage *Nature* **419** 887–9

[89] Bhushan B, Israelachvili J N and Landman U 1995 Nanotribology: friction, wear and lubrication at the atomic scale *Nature* **374** 607–16

[90] Urbakh M *et al* 2004 The nonlinear nature of friction *Nature* **430** 525–8

[91] Schirmeisen A and Schwarz U D 2009 Measuring the friction of nanoparticles: a new route towards a better understanding of nanoscale friction *Chem. Phys. Chem.* **10** 2373–82

[92] Binnig G, Quate C F and Gerber Ch 1986 Atomic force microscope *Phys. Rev. Lett.* **56** 930–3

[93] Giessibl F J 2003 Advances in atomic force microscopy *Rev. Mod. Phys.* **75** 949–83

[94] Geisse N A 2009 AFM and combined optical techniques *Mater. Today* **12** 40–5

[95] Cappella B and Dietler G 1999 Force-distance curves by atomic force microscopy *Surf. Sci. Rep.* **34** 5–104

[96] Butt H, Cappella B and Kappl M 2005 Force measurements with the atomic force microscope: Technique, interpretation and applications *Surf. Sci. Rep.* **59** 1–152

[97] Munz M 2010 Force calibration in lateral force microscopy: a review of the experimental methods *J. Phys. D: Appl. Phys.* **43** 063001

[98] Adrian R J 1991 Particle imaging techniques for experimental fluid mechanics *Annu. Rev. Fluid Mech.* **23** 261–304

[99] Jesuthasan N, Baliga B R and Savage S B 2006 Use of particle tracking velocimetry for measurements of granular flows: Review and application—particle tracking velocimetry for granular flow measurements *Kona* **24** 15–26

[100] Raffel M, Willert C E and Kompenhans J 1998 *Particle Image Velocimetry: A Practical Primer* (New York: Springer)

[101] Ohmi K and Li H Y 2000 Particle-tracking velocimetry with new algorithms *Meas. Sci. Technol.* **11** 603

[102] Kieft R N *et al* 2002 The application of a 3D PTV algorithm to a mixed convection flow *Exp. Fluids* **33** 603–11

[103] Williams D B and Carter C B 2009 *Transmission Electron Microscopy* (New York: Springer) (chapter 1)

[104] Egerton R F 2005 *Physical Principles of Electron Microscopy: An Introduction to TEM, SEM, and AEM* (New York: Springer) (chapters 3 and 4)

[105] Carlton C E and Ferreira P J 2012 *In situ* TEM nanoindentation of nanoparticles *Micron* **43** 1134–9

[106] Altenberger I *et al* 2003 An *in situ* transmission electron microscope study of the thermal stability of near-surface microstructures induced by deep rolling and laser-shock peening *Scr. Mater.* **48** 1593–8

[107] Oshima Y and Kurui Y 2013 In situ TEM observation of controlled gold contact failure under electric bias *Phys. Rev.* B **87** 081404(R)

[108] Cooper K, Gupta A and Beaudoin S 2001 Simulation of the adhesion of particles to surfaces *J. Colloid Interface Sci.* **234** 284–92

[109] Rapaport D C 1997 *The Art of Molecular Dynamics Simulations* (Cambridge: Cambridge University Press)

[110] Dong Y L, Li Q Y and Martini A 2013 Molecular dynamics simulation of atomic friction: A review and guide *J. Vac. Sci. Technol.* A **31** 030801

[111] Steinitz R 1943 The micro-hardness tester—a new tool in powder metallurgy *Met. Alloys* **17** 1183–7

[112] Shorey A B *et al* 1999 Study of material removal during magnetorheological finishing (MRF) *Optical Manufacturing and Testing III* ed H Stahl (Bellingham, WA: SPIE) **3782** 101–11

[113] Chen Y, Mu W B and Lu J X 2012 Young's modulus of PS/CeO_2 composite with core/shell structure microspheres measured using atomic force microscopy *J. Nanopart. Res.* **14** 696

[114] Li J N 2012 Measurements of mechanical properties and removal forces of nanoparticles adhered on silicon substrate *Master Thesis* Tsinghua University, Beijing

[115] Briscoe B J, Fiori L and Pelillo E 1998 Nano-indentation of polymeric surfaces *J. Phys. D: Appl. Phys.* **31** 2395

[116] Tsukruk V V, Shulha H and Zhai X W 2002 Nanoscale stiffness of individual dendritic molecules and their aggregates *Appl. Phys. Lett.* **82** 907–9

[117] Zhang L J and Wang H B 2006 Investigation of the elasticity of polymer nanoparticle by vibrating scanning polarization force microscopy *Chin. Phys. Lett.* **23** 2315–8

[118] Armini S *et al* 2006 Nanoscale indentation of polymer and composite particles by atomic force microscopy *Mater. Res. Soc. Symp. Proc.* **942** W08-03

[119] Zhou J C *et al* 2012 Tuning mechanical properties of liquid crystalline nanoparticles *J. Colloid Interface Sci.* **368** 152–7

[120] Ramos M *et al* 2013 Hardness and elastic modulus on six-fold symmetry gold nanoparticles *Materials* **6** 198–205

[121] Wampler H P and Ivanisevic A 2009 Nanoindentation of gold nanoparticles functionalized with proteins *Micron* **40** 444–8

[122] Saha D R *et al* 2013 Nanoindentation studies on silver nanoparticles *AIP Conf. Proc.* **1536** 257–8

[123] Mook W M *et al* 2007 Compressive stress effects on nanoparticle modulus and fracture *Phys. Rev.* B **75** 214112

[124] Zhang N *et al* 2011 Deformation mechanisms in silicon nanoparticles *J. Appl. Phys.* **109** 063534

[125] Gerbericha W W *et al* 2003 Superhard silicon nanospheres *J. Mech. Phys. Solids* **51** 979–92

[126] Wu B *et al* 2005 Mechanical properties of ultrahigh-strength gold nanowires *Nat. Mater.* **4** 525–9

[127] Jing G Y *et al* 2006 Surface effects on elastic properties of silver nanowires: contact atomic-force microscopy *Phys. Rev.* B **73** 235409

[128] Cuenot S *et al* 2004 Surface tension effect on the mechanical properties of nanomaterials measured by atomic force microscopy *Phys. Rev.* B **69** 165410

[129] Jing G Y, Zhang X Z and Yu D P 2010 Effect of surface morphology on the mechanical properties of ZnO nanowires *Appl. Phys.* A **100** 473–8

[130] Kaplan-Ashiri I et al 2004 Mechanical behavior of individual WS_2 nanotubes *J. Mater. Res.* **19** 454–9

[131] Rothschild A, Cohen S R and Tenne R 1999 WS_2 nanotubes as tips in scanning probe microscopy *Appl. Phys. Lett.* **75** 4025

[132] Zheng M *et al* 2012 Radial mechanical properties of single-walled boron nitride nanotubes *Small* **8** 116–21

[133] Yang Y H and Li W Z 2011 Radial elasticity of single-walled carbon nanotube measured by atomic force microscopy *Appl. Phys. Lett.* **98** 041901

[134] Ebbesen T W 1997 Carbon Nanotubes: Preparation and Properties (New York: CRC)

[135] Minary-Jolandan M and Yu M F 2008 Reversible radial deformation up to the complete flattening of carbon nanotubes in nanoindentation *J. Appl. Phys.* **103** 073516

[136] Jing G Y*et al* 2006 Study of the bending modulus of individual silicon nitride nanobelts via atomic force microscopy *Appl. Phys.* A **82** 475–8

[137] Pakzad A *et al* 2012 Size effects on the nanomechanical properties of cellulose I nanocrystals *J. Mater. Res.* **27** 528–36

[138] Wagner R *et al* 2011 Uncertainty quantification in nanomechanical measurements using the atomic force microscope *Nanotechnology* **22** 455703

[139] Mordehai D *et al* 2011 Nanoindentation size effect in single-crystal nanoparticles and thin films: a comparative experimental and simulation study *Acta Mater.* **59** 2309–21

[140] Mordehai D *et al* 2011 Size effect in compression of single-crystal gold microparticles *Acta Mater* **59** 5202–15

[141] Wang J W *et al* 2013 Atomic-scale dynamic process of deformation-induced stacking fault tetrahedra in gold nanocrystals *Nature Commun.* **4** 2340

[142] Ouyang G *et al* 2012 Atomistic origin of lattice strain on stiffness of nanoparticles *Phys. Chem. Chem. Phys.* **12** 1543–9

[143] Cherian R*et al* 2010 Size dependence of the bulk modulus of semiconductor nanocrystals from first-principles calculations *Phys. Rev.* B **82** 235321

[144] Yang X Y, Xiao S F and Hu W Y 2013 Atomistic simulation for the size effect on the mechanical properties of Ni/Ni_3Al nanowire *J. Appl. Phys.* **114** 094303

[145] Mo Y F, Turner K T and Szlufarska I 2009 Friction laws at the nanoscale *Nature* **457** 1116–9

[146] de Gennes P G, Brochard-Wyart F and Quere D 2002 *Capillarity and wetting phenomena* (New York: Springer)

[147] Barthel E J 2008 Adhesive elastic contacts: JKR and more *J. Phys. D: Appl. Phys.* **41** 163001

[148] Arzt E, Gorb S and Spolenak R 2003 From micro to nano contacts in biological attachment devices *Proc. Natl Acad. Sci. U.S.A.* **100** 10603–6

[149] Liu C *et al* 2012 Hyaluronan and phospholipids in boundary lubrication *Soft Matter* **8** 10241–4

[150] Erlandsson R *et al* 1988 Atomic scale friction between the muscovite mica cleavage plane and a tungsten tip *J. Chem. Phys.* **89** 5190

[151] Larson I *et al* 1993 Direct force measurements between titanium dioxide surfaces *J. Am. Chem. Soc.* **115** 11885–90

[152] Huttl G, Beyer D and Muller E 1997 Investigation of electrical double layers on SiO_2 surfaces by means of force vs. distance measurements *Surf. Interf. Anal.* **25** 543–7

[153] Salameh S *et al* 2012 Adhesion mechanisms of the contact interface of TiO_2 nanoparticles in films and aggregates *Langmuir* **28** 11457–64

[154] Mate C M *et al* 1987 Atomic-scale friction of a tungsten tip on a graphite surface *Phys. Rev. Lett.* **59** 1942–5

[155] Krim J, Solina D H and Chiarello R 1991 Nanotribology of a Kr monolayer: A quartz-crystal microbalance study of atomic-scale friction *Phys. Rev. Lett.* **66** 181–4

[156] Lüthi R *et al* 1994 Sled-type motion on the nanometer scale: determination of dissipation and cohesive energies of c60 *Science* **266** 1979–81

[157] Dietzel D *et al* 2008 Frictional duality observed during nanoparticle sliding *Phys. Rev. Lett.* **101** 125505

[158] Kappl M and Butt H J 2002 The colloidal probe technique and its application to adhesion force measurements *Part. Part. Syst. Charact.* **19** 129–43

[159] Vakarelski I U and Higashitani K 2006 Single-nanoparticle-terminated tips for scanning probe microscopy *Langmuir* **22** 2931–4

[160] Ong Q K and Sokolov I 2007 Attachment of nanoparticles to the AFM tips for direct measurements of interaction between a single nanoparticle and surfaces *J. Colloid Interface Sci.* **310** 385–90

[161] Volkov D O *et al* 2011 Influence of adhesion of silica and ceria abrasive nanoparticles on chemical-mechanical planarization of silica surfaces *Appl. Surf. Sci.* **257** 8518–24

[162] Burtovyy R *et al* 2007 AFM measurements of interactions between CMP slurry particles and substrate *J. Electrochem. Soc.* **154** H476–85

[163] Ramakrishna S N *et al* 2012 Study of adhesion and friction properties on a nanoparticle gradient surface: transition from JKR to DMT contact mechanics *Langmuir* **29** 175–82

[164] Huttl G *et al* 2002 Tailored colloidal AFM probes and their TEM investigation *Surf. Interface Anal.* **33** 50–3

[165] Sokolov I *et al* 2006 AFM study of forces between silica, silicon nitride and polyurethane pads *J. Colloid Interface Sci.* **300** 475–81

[166] Sheehan P E and Lieber C M 1996 Nanotribology and nanofabrication of MoO_3 structures by atomic force microscopy *Science* **272** 1158–61

[167] Dietzel D *et al* 2009 Transition from static to kinetic friction of metallic nanoparticles *Appl. Phys. Lett.* **95** 053104

[168] Landman U *et al* 1990 Atomistic mechanisms and dynamics of adhesion, nanoindentation, and fracture *Science* **248** 454–61

[169] Carpick R W *et al* 1996 Variation of the interfacial shear strength and adhesion of a nanometer-sized contact *Langmuir* **12** 3334–40

[170] Heim L O *et al* 1999 Adhesion and friction forces between spherical micrometer-sized particles *Phys. Rev. Lett.* **83** 3328–31

[171] Ruths M and Granick S 1998 Rate-dependent adhesion between polymer and surfactant monolayers on elastic substrates *Langmuir* **14** 1804–14

[172] Yoshizawa H, Chen Y L and Israelachvili J 1993 Fundamental mechanisms of interfacial friction: I. Relation between adhesion and friction *J. Phys. Chem.* **97** 4128–40

[173] Maeda N *et al* 2002 Adhesion and friction mechanisms of polymer-on-polymer surfaces *Science* **297** 379–82

[174] Greenwood J A and Johnson K L 1981 The mechanics of adhesion of viscoelastic solids *Phil. Mag.* A **43** 697–711

[175] Michel F and Shanahan M E R 1990 Kinetics of the JKR experiment *C. R. Acad. Sci. II* **310** 17–20

[176] Schaefer D M *et al* 1995 Surface roughness and its influence on particle adhesion using atomic force techniques *J. Adhes. Sci. Technol.* **9** 1049–62

[177] Jones R *et al* 2002 Adhesion forces between glass and silicon surfaces in air studied by AFM: effects of relative humidity, particle size, roughness, and surface treatment *Langmuir* **18** 8045–55

[178] Ouyang Q, Ishida K and Okada K 2001 Investigation of micro-adhesion by atomic force microscopy *Appl. Surf. Sci.* **169** 644–8

[179] O'Brien W J and Hermann J J 1973 The strength of liquid bridges between dissimilar materials *J. Adhes.* **5** 91–103

[180] Fisher L R and Israelachvili J N 1981 Experimental studies on the applicability of the Kelvin equation to highly curved concave menisci *J. Colloid Interfce Sci.* **80** 528–41

[181] Christenson H K 1988 Adhesion between surfaces in undersaturated vapors—a reexamination of the influence of meniscus curvature and surface forces *J. Colloid Interface Sci.* **121** 170–8

[182] Batteas J D, Quan X H and Weldon M K 1999 Adhesion and wear of colloidal silica probed by force microscopy *Tribol. Lett.* **7** 121–8

[183] Lesko S *et al* 2001 Investigation by atomic force microscopy of forces at the origin of cement cohesion *Ultramicroscopy* **86** 11–21

[184] Vakarelski I U, Ishimura K and Higashitani K 2000 Adhesion between silica particle and mica surfaces in water and electrolyte solutions *J. Colloid Interface Sci.* **227** 111–8

[185] Vakarelski I U and Higashitani K 2001 Dynamic featuresof shortrange interaction force and adhesion in solutions *J. Colloid Interface Sci.* **242** 110–20

[186] Fuji M *et al* 1999 Effect of wettability on adhesion force between silica particles evaluated by atomic force microscopy measurement asa function of relative humidity *Langmuir* **15** 4584–4

[187] Carrillo J M Y and Dobrynin A V 2012 Dynamics of nanoparticle adhesion *J. Chem.Phys.* **137** 214902

[188] Carrillo J M Y, Raphael E and Dobrynin A V 2010 Adhesion of nanoparticles *Langmuir* **26** 12973–9

[189] Carpick R W*et al* 1996 Measurement of interfacial shear (friction) with an ultrahigh vacuum atomic force microscope *J. Vac. Sci. Technol.* B **14** 1289

[190] Lantz M A *et al* 1997 Atomic-force-microscope study of contact area and friction on $NbSe_2$ *Phys. Rev.* B **55** 10776–85

[191] Schwarz U D *et al* 1997 Quantitative analysis of the frictional properties of solid materials at low loads: I. Carbon compounds *Phys. Rev.* B **56** 6987–96

[192] Gnecco E *et al* 2000 Velocity dependence of atomic friction *Phys. Rev. Lett.* **84** 1172–5

[193] Meyer E *et al* 1996 Site-specific friction force spectroscopy *J. Vac. Sci. Technol.* B **14** 1285

[194] Enachescu M *et al* 1998 Atomic force microscopy study of an ideally hard contact: the diamond(1 1 1)/tungsten carbide interface *Phys. Rev. Lett.* **81** 1877–80

[195] Evstigneev M *et al* 2006 Force dependence of transition rates in atomic friction *Phys. Rev. Lett.* **97** 240601

[196] Zwoner O *et al* 1998 The velocity dependence of frictional forces in point-contact friction *Appl. Phys. A* **66** S263–7

[197] Overney R M *et al* 1994 Anisotropy in friction and molecular stick–slip motion *Phys. Rev. Lett.* **72** 3546–9

[198] Bluhm H *et al* 1995 Anisotropy of sliding friction on the triglycine sulfate (010) surface *Appl. Phys.* A **61** 525–33

[199] Shindo H *et al* 1999 Evidence of the contribution of molecular orientations on the surface force friction of alkaline earth sulfate crystals *Phys. Chem. Chem. Phys.* **1** 1597–600

[200] Park J Y *et al* 2005 High frictional anisotropy of periodic and aperiodic directions on a quasicrystal surface *Science* **309** 1354–6

[201] Schirmeisen A *et al* 2006 Temperature dependence of point contact friction on silicon *Appl. Phys. Lett.* **88** 123108

[202] Zhao X *et al* 2007 Thermally activated friction *Tribol. Lett.* **27** 113–7

[203] Meyer E *et al* 1992 Friction and wear of Langmuir-Blodgett films observed by friction force microscopy *Phys. Rev. Lett.* **69** 1777–80

[204] Overney R M *et al* 1992 Friction measurements on phase-separated thin films with a modified atomic force microscope *Nature* **359** 133–5

[205] Schwarz U D *et al* 1995 Low-load friction behavior of epitaxial C_{60} monolayers under Hertzian contact *Phys. Rev.* B **52** 14976–84

[206] Mougin K *et al* 2008 Manipulation of gold nanoparticles: influence of surface chemistry, temperature, and environment (vacuum versus ambient atmosphere) *Langmuir* **24** 1577–81

[207] Maharaj D and Bhushan B 2012 Effect of spherical Au nanoparticles on nanofriction and wear reduction in dry and liquid environments *Beilstein J. Nanotechnology* **3** 759–72

[208] Sitti M and Hashimoto H 2000 Controlled pushing of nanoparticles: modeling and experiments *IEEE-ASME Trans. Mechatron.* **5** 199–211

[209] Sitti M 2004 Atomic force microcope probe based controlled pushing for nanotribological characterization *IEEE-ASME Trans. Mechatron.* **9** 343–9

[210] Xuan Y and Li Q 2000 Heat transfer enhancement of nanofluids *Int. J. Heat Fluid Flow* **21** 58–64

[211] Eastman J A *et al* 2001 Anomalously increased effective thermal conductivities of ethylene glycol-based nanofluids containing copper nanoparticles *Appl. Phys. Lett.* **78** 718–20

[212] Soppimath K S *et al* 2001 Biodegradable polymeric nanoparticles as drug delivery devices *J. Control. Release* **70** 1–20

[213] Müller R H, Mäder K and Gohla S 2000 Solid lipid nanoparticles (SLN) for controlled drug delivery—a review of the state of the art *Eur. J. Pharm. Biopharm.* **50** 161–77

[214] Xu J *et al* 2005 Atomic scale deformation in the solid surface induced by nanoparticle impacts *Nanotechnology* **16** 859

[215] Luo J and Guo D 2010 Tribology in nanomanufacturing: Interaction between nanoparticles and a solid surface *Adv. Tribol.* 1–5

[216] Si L *et al* 2010 Monoatomic layer removal mechanism in chemical mechanical polishing process: a molecular dynamics study *J. Appl. Phys.* **107** 064310

[217] Bakunin V N *et al* 2004 Synthesis and application of inorganic nanoparticles as lubricant components–a review *J. Nanopart. Res.* **6** 273–84

[218] Shen M W, Luo J B and Wen S Z 2001 The tribological properties of oils added with diamond nano-particles *Tribol. Trans.* **44** 494–8

[219] Nie S and Emory S R 1997 Probing single molecules and single nanoparticles by surface-enhanced Raman scattering *Science* **275** 1102–6

[220] Medintz I L *et al* 2005 Quantum dot bioconjugates for imaging, labelling and sensing *Nature Mater.* **4** 435–46

[221] Greenleaf W J, Woodside M T and Block S M 2007 High-resolution, single-molecule measurements of

biomolecular motion *Annu. Rev. Biophys. Biomol. Struct.* **36** 171–90
[222] Xu X, Luo J and Yan J 2008 A PIV system for two-phase flow with nanoparticles *Int. J. Surf. Sci. Eng.* **2** 168–75
[223] Xu X and Luo J 2007 Marangoni flow in an evaporating water droplet *Appl. Phys. Lett.* **91** 124102
[224] Xu X *et al* 2008 Effect of nanoparticle impact on material removal *Tribol. Trans.* **51** 718–22
[225] Lei J *et al* 2011 Probing particle movement in CMP with fluorescence technique *J. Electrochem. Soc.* **158** H681–5
[226] Lahouij I et *al* 2011 *In situ* TEM observation of the behavior of an individual fullerene-like MoS_2 nanoparticle in a dynamic contact *Tribol. Lett.* **42** 133–40
[227] Zheng H *et al* 2009 Nanocrystal diffusion in a liquid thin film observed by in situ transmission electron microscopy *Nano Lett.* **9** 2460–5
[228] Dai L L, Sharma R and Wu C 2005 Self-assembled structure of nanoparticles at a liquid–liquid interface *Langmuir* **21** 2641–3
[229] Chinas-Castillo F and Spikes H A 2003 Mechanism of action of colloidal solid dispersions *Trans. ASME, J. Tribol.* **125** 552–7
[230] Song B Y *et al* 2003 Study of anti-contact fatigue performance of lubricant with nano silver particle *Lubr. Eng.* **5** 23–6
[231] Yu H L et al 2008 Tribological properties and lubricating mechanisms of Cu nanoparticles in lubricant *Trans. Nonferrous Met. Soc. China* **18** 636–41
[232] Zhang M *et al* Performance and anti-wear mechanism of Cu nanoparticles as lubricating oil additives *Ind. Lubr. Tribol.* **61** 311–8
[233] Zhou J F et al 2000 Tribological behavior and lubricating mechanism of Cu nanoparticles in oil *Tribol. Lett.* **8** 213–8
[234] Qiu S *et al* 2001 Preparation of Ni nanoparticles and evaluation of their tribological performance as potential additives in oils *J. Tribol.* **123** 441–3
[235] Battez A H *et al* 2008 CuO, ZrO_2 and ZnO nanoparticles as antiwear additive in oil lubricants *Wear* **265** 422–8
[236] Battez A H *et al* 2007 Wear prevention behaviour of nanoparticle suspension under extreme pressure conditions *Wear* **263** 1568–74
[237] Ghaednia H, Jackson R L and Khodadadi J M 2013 Experimental analysis of stable CuO nanoparticle enhanced lubricants *J. Exp. Nanosci.* DOI:10.1080/17458080.2013.778424
[238] Gao Y *et al* 2002 Study on tribological properties of oleic acid-modified TiO_2 nanoparticle in water *Wear* **252** 454–8
[239] Radice S and Mischler S 2005 Lubrication properties of Al_2O_3 nanoparticles in aqueous suspensions *Tribol. Interface Eng. Ser.* **48** 101–5
[240] Radice S and Mischler S 2006 Effect of electrochemical and mechanical parameters on the lubrication behaviour of Al_2O_3 nanoparticles in aqueous suspensions *Wear* **261** 1032–41
[241] Sun L *et al* 2004 Synthesis and characterization of DDP coated Ag nanoparticles *Mater. Sci. Eng.* A **379** 378–83
[242] Sun L *et al* 2010 Synthesis and tribology properties of stearate-coated Ag nanoparticles *Tribol. Trans.* **53** 174–8
[243] Twist C P et al 2012 Molecularly-engineered lubricants: synthesis, activation, and tribological characterization of silver complexes as lubricant additives *Adv. Eng. Mater.* **14** 101–5
[244] Greenberg R *et al* 2004 The effect of WS_2 nanoparticles on friction reduction *Tribol. Lett.* **17** 179–86
[245] Rapoport L *et al* 2003 Tribological properties of WS_2 nanoparticles under mixed lubrication *Wear* **255** 785–93
[246] Tevet O *et al* 2011 Friction mechanism of individual multilayered nanoparticles *Proc. Natl Acad. Sci. USA* **108** 19901–6
[247] Cizaire L *et al* 2002 Mechanisms of ultra-low friction by hollow inorganic fullerene-like MoS_2 nanoparticles *Surf. Coat. Technol.* **160** 282–7
[248] Rosentsveig R *et al* 2009 Fullerene-like MoS_2 nanoparticles and their tribological behavior *Tribol. Lett.* **36** 175–82
[249] Yang J H *et al* 2008 Synthesis and tribological properties of WSe_2 nanorods *Nano. Res. Lett.* **3** 481–5
[250] Xu T, Zhao J Z and Xu K 1996 The ball-bearing effect of diamond nanoparticles as an oil additive *J. Phys. D: Appl. Phys.* **29** 2932
[251] Chu H Y, Hsu W C and Lin J F 2010 The anti-scuffing performance of diamond nano-particles as an oil additive *Wear* **268** 960–7
[252] Chou C C and Lee S H 2008 Rheological behavior and tribological performance of a nanodiamond-dispersed lubricant *J. Mater. Process. Technol.* **201** 542–7
[253] Lee C G *et al* 2009 Study on the tribological characteristics of graphite nano lubricants *Int. J. Precis. Eng. Manuf.* **10** 85–90
[254] Chen Q *et al* 2013 Preparation of water-soluble nanographite and its application in water-based cutting fluid *Nanoscale Res. Lett.* **8** 52
[255] Ginzburg B M *et al* 2002 Antiwear effect of fullerene C60 additives to lubricating oils *Russ. J. Appl. Chem.* **75** 1357–62
[256] Lee J *et al* 2007 Enhancement of lubrication properties of nano-oil by controlling the amount of fullerene nanoparticle additives *Tribol. Lett.* **28** 203–8
[257] Ku B C *et al* 2010 Tribological effects of fullerene (C60) nanoparticles added in mineral lubricants according to its viscosity *Int. J. Precis. Eng. Manuf.* **11** 607–11
[258] Li X H *et al* 2006 Surface-modification in situ of nano-SiO_2 and its structure and tribological properties *Appl. Surf. Sci.* **252** 7856–61
[259] Peng D X et al 2009 Tribological properties of diamond and SiO_2 nanoparticles added in paraffin *Tribol. Int.* **42** 911–7
[260] Peng D X *et al* 2010 Size effects of SiO_2 nanoparticles as oil additives on tribology of lubricant *Ind. Lubr. Tribol.* **62** 111–20
[261] Kheireddin B A *et al* 2013 Inorganic nanoparticle-based ionic liquid lubricants *Wear* **303** 185–90
[262] Jia D *et al* 2011 The tribology properties of alumina/silica composite nanoparticles as lubricant additives *Appl. Surf. Sci.* **257** 5720–5
[263] Rico E F, Minondo I and Cuervo D G 2007 The effectiveness of PTFE nanoparticle powder as an EP additive to mineral base oils *Wear* **262** 1399–406
[264] Rico E F, Minondo I and Cuervo D G 2009 Rolling contact fatigue life of AISI 52100 steel balls with mineral and synthetic polyester lubricants with PTFE nanoparticle powder as an additive *Wear* **266** 671–7
[265] Si L N *et al* 2011 Abrasive rolling effects on material removal and surface finish in chemical mechanical polishing analyzed by molecular dynamics simulation *J. Appl. Phys.* **109** 084335
[266] Luo J F and Dornfeld D A 2001 Material removal mechanism in chemical mechanical polishing: theory and modeling *IEEE Trans. Semicond. Manuf.* **14** 112–33
[267] Seok J *et al* 2003 Multiscale material removal modeling of chemical mechanical polishing *Wear* **254** 307–20
[268] Basak A K *et al* 2010 Material removal mechanisms of monocrystalline silicon under the impact of high velocity micro-particles *Wear* **3–4** 269–77

[269] Duan F L *et al* 2005 Atomistic structural change of silicon surface under a nanoparticle collision *Chin. Sci. Bull.* **50** 1661–5

[270] Chen R L *et al* 2008 Extrusion formation mechanism on silicon surface under the silica cluster impact studied by molecular dynamics simulation *J. Appl. Phys.* **104** 104907

[271] Chen R L *et al* 2009 Energy transfer under impact load studied by molecular dynamics simulation *J. Nanopart. Res.* **11** 589–600

[272] Liang H, Le Mogne T and Martin J M 2002 Interfacial transfer between copper and polyurethane in chemical-mechanical polishing *J. Electron. Mater.* **31** 872–8

[273] Liang H and Xu G H 2002 Lubricating behavior in chemical-mechanical polishing of copper *Scr. Mater.* **46** 343–7

[274] Paul E *et al* 2007 A model of pad-abrasive interactions in chemical mechanical polishing *Electrochem. Solid State* **10** H131–3

[275] Ahmadi G and Xia X 2001 A model for mechanical wear and abrasive particle adhesion during the chemical mechanical polishing process *J. Electrochem. Soc.* **148** G99–109

[276] Zhao Y W and Chang L 2002 A micro-contact and wear model for chemical-mechanical polishing of silicon wafers *Wear* **252** 220–6

[277] Levert J A *et al* 1998 Mechanisms of chemical-mechanical polishing of SiO_2 dielectric on integrated circuits *Tribol. Trans.* **41** 593–9

[278] Zhou C H *et al* 2002 Influence of colloidal abrasive size on material removal rate and surface finish in SiO2 chemical mechanical polishing *Tribol. Trans.* **45** 232–8

[279] Zhang F and Busnaina A 1998 The role of particle adhesion and surface deformation in chemical mechanical polishing processes *Electrochem. Solid St.* **1** 184–7

[280] Ng D 2007 Interfacial forces in chemical-mechanical polishing(CMP) Texas A&M University Dissertation December 2007.

[281] Busnaina A A *et al* 2000 Surface cleaning mechanisms and future cleaning requirements *IEEE/SEMI Advanced Semiconductor Manufacturing Conf. Workshop (Boston, MA)* pp 328–33

[282] Busnaina A A *et al* 2002 Particle adhesion and removal mechanisms in post-CMP cleaning processes *IEEE Trans. Semicond. Manuf.* **15** 374–82

[283] Thoreson E J, Martin J and Burnham N A 2006 The role of few-asperity contacts in adhesion *J. Colloid Interface Sci.* **298** 94–101

[284] Lei J 2011 Experimental study of particle movement and adhesion in chemical mechanical planarization *Master thesis* Tsinghua University Beijing.

[285] Burdick G M, Berman N S and Beaudoin S P 2001 Describing hydrodynamic particle removal from surfaces using the particle Reynolds number *J. Nanoparticle Res.* **3** 455–67

[286] Liu C W, Dai B T and Yeh C F 1996 Post cleaning of chemical mechanical polishing process *Appl. Surf. Sci.* 92 176–9

[287] Martinez M A 1994 Chemical-mechanical polishing-route to global planarization *Solid State Technol.* **37** 26–31

[288] Huang Y T *et al* 2011 Mechanisms for nano particle removal in brush scrubber cleaning *Appl. Surf. Sci.* **257** 3055–62

[289] An J *et al* 2012 Effect of process parameters on particle removal efficiency in poly(vinyl alcohol) brush scrubber cleaning *Japan. J. Appl. Phys.* **51** 026501

[290] Huang Y T *et al* 2011 Modeling of particle removal processes in brush scrubber cleaning *Wear* **273** 105–11

[291] Huang Y T *et al* 2011 A lubrication model between the soft porous brush and rigid flat substrate for post-CMP cleaning *Microelectron. Eng.* **8** 2862–70

[292] Kim H, Lee Y and Lim E 2013 Development of a near-field megasonic cleaning system for nano-particle removal *Solid State Phenom.* **195** 205–8

[293] Bakhtari K *et al* 2006 Experimental and numerical investigation of nanoparticle removal using acoustic streaming and the effect of time *J. Electrochem. Soc.* **153** G846–50

[294] Busnaina A A and Elsawy T M 1998 Post-CMP cleaning using acoustic streaming *J. Electron. Mater.* **27** 1095–8

[295] Huang Y T *et al* 2009 Particles detection and analysis of hard disk substrate after cleaning of post chemical mechanical polishing *Appl. Surf. Sci.* **255** 9100–4

[296] Ng D *et al* 2007 Nanoparticle removal mechanisms during post-CMP cleaning *Electrochem. Solid-State Lett.* **10** H227–31

[297] ILIE F and TITA C 2009 Interaction between nanoparticles during chemical mechanical polishing (CMP) *Optoelectron. Adv. Mater.* **3** 245–8

[298] Gholivand K *et al* 2010 A novel surface cleaning method for chemical removal of fouling lead layer from chromium surfaces *Appl. Surf. Sci.* **256** 7457–61

[299] Ng D *et al* 2008 Role of surfactant molecules in post-CMP cleaning *J. Electrochem. Soc.* **155** H64–8

[300] Lin J C *et al* 2006 Mechanical behavior of various nanoparticle filled composites at low-velocity impact *Compos. Struct.* **74** 30–6

[301] Kang Y C and Chan S L 2004 Tensile properties of nanometric Al_2O_3 particulate-reinforced aluminum matrix composites *Mater. Chem. Phys.* **85** 438–43

[302] Liu Y Q *et al* 2009 AlN nanoparticle-reinforced nanocrystalline Al matrix composites: Fabrication and mechanical properties *Mater. Sci. Eng.* A **505** 151–6

[303] Baghchesara M A and Abdizadeh H 2012 Microstructural and mechanical properties of nanometric magnesium oxide particulate-reinforced aluminum matrix composites produced by powder metallurgy method *J Mech. Sci. Technol.* **26** 367–72

[304] Shao W *et al* 2012 Mechanical and corrosion resistance properties of TiO_2 nanoparticles reinforced Ni coating by electrodeposition *IOP Conf. Ser.: Mater. Sci. Eng.* **40** 012043

[305] Indyka P, Beltowska-Lehman E and Bigos A 2012 Microstructural characterisation of electrodeposited coatings of metal matrix composite with alumina nanoparticles *IOP Conf. Series. Mater. Sci. Eng.* **32** 012010

[306] Levashov E, Kurbatkina V and Alexandr Z 2010 Improved mechanical and tribological properties of metal-matrix composites dispersion-strengthened by nanoparticles *Materials* **3** 97–109

[307] Shen J H *et al* 2013 Effect of ceramic nanoparticle reinforcements on the quasistatic and dynamic mechanical properties of magnesium-based metal matrix composites *J. Mater. Res.* **28** 1835–52

[308] Wang Z H *et al* 2010 SiC nanoparticles reinforced magnesium matrix composites fabricated by ultrasonic method *Trans. Nonferrous. Met. Soc. China* **20** s1029–32

[309] Rajkumar K and Aravindan S 2013 Tribological behavior of microwave processed copper-nanographite composites *Tribol. Int.* **57** 282–96

[310] Sabagh S, Bahramian A R and Kokabi M 2012 SiAlON nanoparticles effect on the behaviour of epoxy coating *Iran Polym. J.* **21** 229–37

[311] Ahmad T, Mamat O and Ahmad R 2013 Studying the effects of adding silica sand nanoparticles on epoxy based composites *J. Nanoparticles* **2013** 603069

[312] Li J H *et al* 2009 Effects of ZnO nanoparticles on the mechanical and antibacterial properties of polyurethane coatings *Prog. Org. Coat.* **64** 504–9
[313] Wang H Y *et al* 2011 Effect of grafted polytetrafluoroethylene nanoparticles on the mechanical and tribological performances of phenol resin *Mater. Sci. Eng. A* **528** 6878–86
[314] Sun L H, Yang Z G and Li X H 2008 Mechanical and tribological properties of polyoxymethylene modified with nanoparticles and solid lubricants *Polymer Eng. Sci.* **48** 1824–32
[315] Rohatgi P K and Schultz B 2007 Lightweight metal matrix nanocomposites-stretching the boundaries of metals *Mater. Matters* **2.4** 16
[316] Muralidhara H B *et al* 2012 Electrodeposition of Zn-Graphite nanoparticles composite and their characterization *J. Chem. Pharm. Res.* **4** 440–9
[317] Bakshi S R, Lahiri D and Agarwal A 2010 Carbon nanotube reinforced metal matrix composites—a review *Int. Mater. Rev.* **55** 41–64
[318] Hanemann T and Vinga Szabó D 2010 Polymer–nanoparticle composites: from synthesis to modern applications *Materials* **3** 3468–517
[319] Shi X M *et al* 2009 Effect of nanoparticles on the anticorrosion and mechanical properties of epoxy coating *Surf. Coat. Technol.* **204** 237–45
[320] Burris D L 2007 Effects of nanoparticles on the wear resistance of polytetrafluoroethylene *Doctoral Thesis* University of Florida
[321] Ramezanzadeha B, Attara M M, Farzamb M 2011 A study on the anticorrosion performance of the epoxy-polyamide nanocomposites containing ZnO nanoparticles *Prog. Org. Coat.* **72** 410–22
[322] Tjong S C 2007 Novel nanoparticle-reinforced metal matrix composites with enhanced mechanical properties *Adv. Eng. Mater.* **9** 639–52
[323] Guo Y B, Wang D G and Liu S H 2010 Tribological behavior of in situ Ag nanoparticles/polyelectrolyte composite molecular deposition films *Appl. Surf. Sci.* **256** 1714–9
[324] Guo Y B, Wang D G and Zhang S W 2011 Adhesion and friction of nanoparticles/polyelectrolyte multilayer films by AFM and micro-tribometer *Tribol. Int.* **44** 906–15
[325] Hakim L F *et al* 2007 Nanoparticle coating for advanced optical, mechanical and rheological properties *Adv. Funct. Mater.* **17** 3175–81
[326] Wang J, Shi T J and Jiang X C 2008 Synthesis and characterization of core–shell ZrO_2/PAAEM/PS nanoparticles *Nanoscale Res. Lett.* **4** 240–6